



**NAVAL  
POSTGRADUATE  
SCHOOL**

**MONTEREY, CALIFORNIA**

**THESIS**

**FABRICATION OF A MECHANICALLY ROBUST  
CARBON NANOFIBER FOAM**

by

William J. Curtin

June 2015

Thesis Advisor:

Claudia Luhrs

Second Reader:

Garth Hobson

**Approved for public release; distribution is unlimited**

THIS PAGE INTENTIONALLY LEFT BLANK

<b>REPORT DOCUMENTATION PAGE</b>			<i>Form Approved OMB No. 0704-0188</i>
Public reporting burden for this collection of information is estimated to average 1 hour per response, including the time for reviewing instruction, searching existing data sources, gathering and maintaining the data needed, and completing and reviewing the collection of information. Send comments regarding this burden estimate or any other aspect of this collection of information, including suggestions for reducing this burden, to Washington headquarters Services, Directorate for Information Operations and Reports, 1215 Jefferson Davis Highway, Suite 1204, Arlington, VA 22202-4302, and to the Office of Management and Budget, Paperwork Reduction Project (0704-0188) Washington, DC 20503.			
<b>1. AGENCY USE ONLY (Leave blank)</b>	<b>2. REPORT DATE</b> June 2015	<b>3. REPORT TYPE AND DATES COVERED</b> Master's Thesis	
<b>4. TITLE AND SUBTITLE</b> FABRICATION OF A MECHANICALLY ROBUST CARBON NANOFIBER FOAM		<b>5. FUNDING NUMBERS</b>	
<b>6. AUTHOR(S)</b> William J. Curtin			
<b>7. PERFORMING ORGANIZATION NAME(S) AND ADDRESS(ES)</b> Naval Postgraduate School Monterey, CA 93943-5000		<b>8. PERFORMING ORGANIZATION REPORT NUMBER</b>	
<b>9. SPONSORING /MONITORING AGENCY NAME(S) AND ADDRESS(ES)</b> N/A		<b>10. SPONSORING/MONITORING AGENCY REPORT NUMBER</b>	
<b>11. SUPPLEMENTARY NOTES</b> The views expressed in this thesis are those of the author and do not reflect the official policy or position of the Department of Defense or the U.S. government. IRB Protocol number ___N/A___.			
<b>12a. DISTRIBUTION / AVAILABILITY STATEMENT</b> Approved for public release distribution is unlimited		<b>12b. DISTRIBUTION CODE</b> A	
<b>13. ABSTRACT (maximum 200 words)</b>  In this thesis, the constrained formation of fibrous nanostructures process was scaled up to fabricate mechanically robust, homogenous foam samples. Scaling up this process required the design of a stainless steel mold capable of maintaining conditions supportive of the carbon nanofiber foam growth such as gas flows, constrained growth area, stable at the temperature and time employed. The gas flow distribution during the growth process was achieved using stainless steel deflectors capable of consistently directing adequate amounts of hydrocarbon to all chamber regions. ANSYS CFX models were used to simulate the gas flows with and without deflectors. Analysis of the experimental variables impact on the foam generation showed that the gas flows and their temperature had a greater influence in the foam robustness than reaction times. Control over the growth variables successfully created an interwoven carbon nanofiber foam material of larger dimensions than previous efforts. The carbon mats microstructures were studied using Scanning Electron Microscopy and their surface area determined by the Brunauer-Emmett-Teller method. The catalyst employed during fabrication was recovered using a leaching method that dissolved the palladium without damaging the carbon foam. The recovery experiment validated the technique as a viable way to reduce manufacturing costs in this process.			
<b>14. SUBJECT TERMS</b> Mechanically robust nanofiber foam production method		<b>15. NUMBER OF PAGES</b> 81	
		<b>16. PRICE CODE</b>	
<b>17. SECURITY CLASSIFICATION OF REPORT</b> Unclassified	<b>18. SECURITY CLASSIFICATION OF THIS PAGE</b> Unclassified	<b>19. SECURITY CLASSIFICATION OF ABSTRACT</b> Unclassified	<b>20. LIMITATION OF ABSTRACT</b> UU

NSN 7540-01-280-5500

Standard Form 298 (Rev. 2-89)  
Prescribed by ANSI Std. Z39-18

THIS PAGE INTENTIONALLY LEFT BLANK

**Approved for public release; distribution is unlimited**

**FABRICATION OF A MECHANICALLY ROBUST NANOFIBER FOAM**

William J. Curtin  
Lieutenant, United States Navy  
B.S., University of Idaho, 2008

Submitted in partial fulfillment of the  
requirements for the degree of

**MASTER OF SCIENCE IN MECHANICAL ENGINEERING**

from the

**NAVAL POSTGRADUATE SCHOOL  
June 2015**

Author: William J. Curtin

Approved by: Claudia Luhrs  
Thesis Advisor

Garth Hobson  
Second Reader

Garth Hobson  
Chair, Department of Mechanical and Aerospace Engineering

THIS PAGE INTENTIONALLY LEFT BLANK

## **ABSTRACT**

In this thesis, the constrained formation of fibrous nanostructures process was scaled up to fabricate mechanically robust, homogenous foam samples. Scaling up this process required the design of a stainless steel mold capable of maintaining conditions supportive of the carbon nanofiber foam growth such as gas flows, constrained growth area, stable at the temperature and time employed. The gas flow distribution during the growth process was achieved using stainless steel deflectors capable of consistently directing adequate amounts of hydrocarbon to all chamber regions. ANSYS CFX models were used to simulate the gas flows with and without deflectors. Analysis of the experimental variables impact on the foam generation showed that the gas flows and their temperature had a greater influence in the foam robustness than reaction times. Control over the growth variables successfully created an interwoven carbon nanofiber foam material of larger dimensions than previous efforts. The carbon mats' microstructures were studied using scanning electron microscopy and their surface area determined by the Brunauer-Emmett-Teller method. The catalyst employed during fabrication was recovered using a leaching method that dissolved the palladium without damaging the carbon foam. The recovery experiment validated the technique as a viable way to reduce manufacturing costs in this process.

THIS PAGE INTENTIONALLY LEFT BLANK

# TABLE OF CONTENTS

<b>I.</b>	<b>INTRODUCTION.....</b>	<b>1</b>
	A. <b>MOTIVATION .....</b>	<b>1</b>
	B. <b>PERSONAL PROTECTIVE MATERIALS .....</b>	<b>1</b>
	C. <b>WHY CARBON NANOFIBER FOAMS? .....</b>	<b>2</b>
	D. <b>EARLIER RESEARCH EFFORTS.....</b>	<b>2</b>
	E. <b>THESIS OUTLINE.....</b>	<b>3</b>
	1. <b>Objectives.....</b>	<b>3</b>
	2. <b>Hypotheses .....</b>	<b>3</b>
	3. <b>Tasks.....</b>	<b>4</b>
	4. <b>Contributions of This Work.....</b>	<b>4</b>
<b>II.</b>	<b>EXPERIMENTAL METHODS .....</b>	<b>5</b>
	A. <b>MOLD DESIGN.....</b>	<b>5</b>
	B. <b>CARBON NANOFIBER PRODUCTION.....</b>	<b>8</b>
	1. <b>Experimental Setup Procedures .....</b>	<b>8</b>
	a. <i>Cleanliness/Lubrication.....</i>	<i>8</i>
	b. <i>Setup/Palladium Placement.....</i>	<i>9</i>
	c. <i>Gas Mixture.....</i>	<i>12</i>
	C. <b>DESIGN SCALE UP.....</b>	<b>12</b>
	1. <b>Preliminary CFF Experiments .....</b>	<b>12</b>
	2. <b>Modification of Scale Up Experiment Variables to Produce Larger Mat .....</b>	<b>13</b>
	a. <i>Palladium .....</i>	<i>13</i>
	b. <i>Gas flow .....</i>	<i>14</i>
	c. <i>Temperature .....</i>	<i>14</i>
	3. <b>Utilization of Gas Flow Deflectors.....</b>	<b>15</b>
	a. <i>Rod Deflector ONE .....</i>	<i>16</i>
	b. <i>Foil Deflector ONE.....</i>	<i>16</i>
	c. <i>Foil Deflector TWO .....</i>	<i>17</i>
	d. <i>Foil Deflector THREE.....</i>	<i>18</i>
	e. <i>Foil Deflector FOUR.....</i>	<i>19</i>
	f. <i>Foil Deflector FIVE.....</i>	<i>19</i>
	g. <i>Foil Deflector SIX.....</i>	<i>20</i>
	D. <b>CATALYST RECOVERY.....</b>	<b>21</b>
	E. <b>CHARACTERIZATION METHODS .....</b>	<b>22</b>
	1. <b>Scanning Electron Microscopy (SEM) and Back-Scattered Electron Signal (BSE).....</b>	<b>22</b>
	2. <b>Brunauer-Emmett-Teller (BET) Characterization .....</b>	<b>23</b>
<b>III.</b>	<b>RESULTS AND DISCUSSION .....</b>	<b>25</b>
	A. <b>FIBER GROWTH .....</b>	<b>25</b>
	B. <b>CONSTRAINED FORMATION OF FIBROUS NANOSTRUCTURES.....</b>	<b>27</b>

1.	Precursors Gases.....	28
2.	Catalysts.....	28
3.	Temperature.....	29
C.	GROWTH MODEL THEORY .....	29
D.	CATALYST RECOVERY DISCUSSION .....	30
E.	FOAM ANALYSIS .....	31
1.	Preliminary CFF Experiment.....	31
2.	CFF Experiment: Without Deflector .....	33
3.	CFF Experiment: Rod Deflector ONE.....	36
4.	CFF Experiment: Foil Deflector ONE .....	37
5.	CFF Experiment: Foil Deflector TWO .....	39
6.	CFF Experiment: Foil Deflector THREE.....	40
7.	CFF Experiment: Foil Deflector FOUR .....	42
8.	CFF Experiment: Foil Deflector FIVE .....	44
9.	CFF Experiment: Foil Deflector SIX .....	46
F.	CATALYST RECOVERY: SUMMARY OF FINDINGS .....	50
1.	Interior region analysis.....	51
2.	Exterior region analysis.....	52
IV.	CONCLUSION .....	53
	APPENDIX.....	55
	LIST OF REFERENCES.....	57
	INITIAL DISTRIBUTION LIST .....	61

## LIST OF FIGURES

Figure 1.	CFF mold chamber with attached inlet and outlet connections.....	6
Figure 2.	CNC machine creating the main CFF growth chamber.....	7
Figure 3.	Finalized chamber for CFF growth. The figure shows the path traveled by the gases through the mold. ....	7
Figure 4.	Palladium arrangement (0.5 gram) within the main mold chamber. ....	9
Figure 5.	LindBerg Blue M model BF51442C furnace shown from the front with chamber door closed and window packing material in place. ....	10
Figure 6.	Interior chamber shown with the door open from the front.....	10
Figure 7.	MKS mass flow controller (model MKS 647a).....	11
Figure 8.	Erlenmeyer exhaust trap utilizing zeolite and permanganate. ....	11
Figure 9.	Early CFF experimental mold (dimensions of 0.5 x 0.344 x 2.25 inches) shown with 0.02 grams of palladium distributed within the chamber. ....	13
Figure 10.	Increased chamber inlet length shown attached to the scaled mold. ....	15
Figure 11.	ANSYS modeling of the mold chamber shows the flow velocities along within the chamber.....	15
Figure 12.	Image showing the length of Deflector ONE. ....	16
Figure 13.	Image showing foil deflector base in position within the chamber. ....	17
Figure 14.	Foil Deflector TWO in position within the chamber. ....	18
Figure 15.	Foil Deflector THREE in position within the chamber. ....	18
Figure 16.	Foil Deflector FOUR in position within the chamber. ....	19
Figure 17.	Foil Deflector FIVE in position within the chamber. ....	20
Figure 18.	Foil Deflector SIX in position within the chamber.....	20
Figure 19.	Zeiss Neon 40 electron microscope. ....	22
Figure 20.	Nova 4200e. ....	23
Figure 21.	The carbon nanofoam shown in image a, has carbon structures ranging from 1–10 nm in diameter. These structures appear to be assembled in a highly chaotic and unorganized formation. The carbon nanofibers shown in image b have structures ranging from 100 - 300 nm in diameter. The individual fibers shown in this image all have the typical symmetric cylindrical appearance. The carbon structure shown in image c on the other hand is the largest of the three image structures. The diameters of these structures are measured in microns which is several orders of magnitude larger than the structures seen in image a and b, from [16, 20, 22] .....	27
Figure 22.	Depictions of the “tip-growth” (a) and “base growth” (b) models showing the vapor-liquid-solid growth process, from [8]. ....	30
Figure 23.	Preliminary CFF Experiment prior to its removal from the chamber.....	31
Figure 24.	Image of foam after removal from the chamber. ....	31
Figure 25.	CFF diameter size distribution of the preliminary experimental results used as a comparison against other experimental results.....	32
Figure 26.	SEM and BSE taken of foam at 7.5K magnification. The bright regions show the palladium the remains within the foam after growth.....	32

Figure 27.	Scaled CFF experiment images showing the results after opening the main chamber.....	34
Figure 28.	Left image shows an SEM image taken of the foam experiment that utilized no deflector. Right image is a BSE image taken of the same experimental results. ....	34
Figure 29.	Left image shows foam after removal from the main chamber. Right image shows and (right) a comparison between the non-deflected (A) and deflected (B) experiments. ....	36
Figure 30.	Left image shows an SEM image taken of the foam from Rod Deflector ONE experiment. Right image is a BSE image taken of the same experimental results. ....	37
Figure 31.	Image taken of the results from Foil Deflector ONE’s experiment after the main chamber was opened. ....	38
Figure 32.	Left image shows an SEM image taken of the foam from Foil Deflector ONE’s experiment. Right image is a BSE image taken of the same experimental results. ....	38
Figure 33.	Left image shows Foil Deflector TWO’s experiment after opening of the main chamber. Right shows the main chamber after the removal of Foil Deflector TWO. ....	40
Figure 34.	Left image shows an SEM image taken of the foam from Foil Deflector TWO’s experiment. Right image is a BSE image taken of the same experimental results. ....	40
Figure 35.	Left image shows Foil Deflector THREE’s experiment after opening of the main. Right image shows the CFF generated during the process. ....	41
Figure 36.	SEM image taken from sample 103014.....	42
Figure 37.	Left image shows Foil Deflector FOUR’s experiment after opening of the main chamber. Right image shows the removed CFF block after removal from the main chamber. ....	43
Figure 38.	Left image shows an SEM image taken of the foam from Foil Deflector FOUR’s experiment. Right image is a BSE image taken of the same experimental results. ....	43
Figure 39.	Smaller fiber diameters observed due to the inclusion of tungsten oxide. ....	44
Figure 40.	Left image shows Foil Deflector FIVE’s experiment after opening of the main chamber. Right image shows the removed foam block after removal from the main chamber. ....	45
Figure 41.	Left image shows an SEM image taken of the foam from Foil Deflector FIVE’s experiment. Right image is a BSE image taken of the same experimental results. ....	46
Figure 42.	ANSYS modeling of the mold chamber utilizing Foil Deflector SIX shows the modified flow paths within the chamber.....	47
Figure 43.	Left image shows the completely disassembled Deflector SIX from the experiment. Right image shows a rear view of the assembled deflector. ....	48
Figure 44.	Image shows Foil Deflector SIX experiment growth after opening of the main chamber.....	48

Figure 45.	Left image shows a forward view of the CFF block generated during Foil Deflector SIX's experiment and placed atop the main chamber after removal. Right image shows a rear view of the results. ....	48
Figure 46.	SEM and BSE images taken from a sample of the CFF block generated in Foil Deflector SIX's experiment.....	49
Figure 47.	Consolidated diameter distribution results from all CFF experiments. ....	50
Figure 48.	BSE images taken of samples after the palladium recovery procedure. Left image shows solution 1 sample and right image shows solution 2 sample. ...	51
Figure 49.	Palladium catalyst particle size distribution of the interior region of sample specimen taken after recovery method procedure. ....	51
Figure 50.	Palladium catalyst particle size distribution of the exterior region of sample specimen taken after recovery method procedure. ....	52
Figure 51.	SOLIDWORKS renderings of the new mold chamber design. ....	55

THIS PAGE INTENTIONALLY LEFT BLANK

## LIST OF TABLES

Table 1.	Experimental gas flows used for experiments. ....	14
Table 2.	Summary of all experimental variables. ....	49

THIS PAGE INTENTIONALLY LEFT BLANK

## LIST OF ACRONYMS AND ABBREVIATIONS

BET	Brunauer-Emmett-Teller
BSE	Back-Scattered Electron
CNC	Computerized Numerical Control
CNF	Carbon Nanofiber
CFF	Carbon Nanofiber Foam
CNT	Carbon Nanotube
CVD	Chemical Vapor Deposition
CoFFiN	Constrained Formation of Fibrous Nanostructures
GPa	Giga-Pascal
HOPG	Highly Oriented Pyrolytic Graphite
IBA	Interceptor Body Armor
KPa	Kilo-Pascal
MFC	Mass Flow Controller
MPa	Mega-Pascal
MWCNT	Multi-wall Carbon Nanotubes
nm	Nanometer
No	Number
Pd	Palladium
PSI	Pounds per square inch
SCCM	Standard Cubic Centimeter
SEM	Secondary Electron Microscopy
SWCNT	Single-wall carbon nanotube
TGA	Thermal Graphic Analysis
UHP	Ultra High Purity

THIS PAGE INTENTIONALLY LEFT BLANK

## ACKNOWLEDGMENTS

To my advisor, Dr. Claudia Luhrs, thank you so much for all the guidance and support you have provided to me during my time here at NPS. You are the most motivating professor that I have had an opportunity to learn from at this institution. Your ability to engage nanomaterial and present it from multiple different points of view not only improved my understanding of the material but also drove my interest in the topic. I wish you continued achievement in your career.

To Dr. Sarath Menon, thank you for your efforts and patience with me while training me to use the SEM. Without your extra effort, I could not have accomplished nearly so much in this research as I was able to.

To Pedro Arias, your efforts with experimental setup and data collection produced a direct and significant positive influence over the entirety of this work. I appreciate your time and friendship and wish you success with all your future endeavors.

I would also like to thank Dr. Chanman Park for assisting with equipment setup. I also want to recognize John Mobley, who operated the CNC mill during the fabrication of the main growth chamber. Without your help, I would not have been able to complete the thesis.

I also want to thank my wonderful wife, Amanda, and our two children, Emily and Jacob. You mean the world to me. Your continuing love and support keeps me energized as well as lifts my spirits.

THIS PAGE INTENTIONALLY LEFT BLANK

# **I. INTRODUCTION**

## **A. MOTIVATION**

The primary motivation of this research was to determine the conditions necessary to enable the scalability of carbon nanofiber foam (CFF) production. We aimed to produce a homogenous, mechanically robust sample, which dimensions were of at least 5 x 4 x 0.5 inches. The sample size specifications provided by the Office of Naval Research, were selected to meet the minimum size required to make practical its testing using NATO rounds. This testing would lead to a feasibility determination of whether CFFs could improve the performance of bulletproof personal protection systems.

## **B. PERSONAL PROTECTIVE MATERIALS**

The wars in both Afghanistan and Iraq have demonstrated the importance of personnel and vehicle protective systems. Advances in the design of these systems have saved lives and resources by stopping penetrators from reaching both vital organs and sensitive equipment in combat zones. The trade-off for this improved protection has been the increased weight on soldiers and systems. For example, the interceptor body armor used by the U.S. Army in Afghanistan weighed more than 30 pounds, accounting for over 30% of the soldiers' weight-carrying limit [1]. This weight restricts the body's freedom of movement while also slowing the soldier down. Both effects increase the service member's susceptibility in combat. The continued objective to further the creation of lighter, stronger, and more durable protective systems is the ultimate aim of this research.

The dilemma often faced in the creation of protection systems, is that improvements in performance often result in increased weight. A possible solution to this problem lies in the replacement of bulkier shock-absorbing materials with ultra-low density, carbon nanofiber foams. CFFs are formed from a catalyst reaction with a carbon source, which creates nanofibers. These fibers can range in diameter from a few to hundreds of nanometers (nm) in diameter. Despite their small size, these new materials have been shown to have incredible properties. Thus, what this thesis describes is the

development of a CFF mat that could be used as backing material along currently employed ballistic fabrics.

### **C. WHY CARBON NANOFIBER FOAMS?**

Carbon nanofiber foam (CFF) has been shown to possess several unique properties that would be advantageous to exploit. CFF has excellent shock-absorbing properties. Research conducted to study the shock-dampening properties of single-walled carbon nanotubes (SWCNT) showed an ability to withstand fracture stresses of 6.3 MPa under 60% strain [2]. Other studies utilizing CFFs have created hybrid materials composed of CFF and epoxies. A CFF weight loading of 1% of that of the epoxies weight was shown to improve the Young's modulus of the epoxy by greater than 100% [3]. CFFs are extremely light, having measured densities of only 0.125 g/cm<sup>3</sup> [4], and are thermally stable. Thermal graphic analysis (TGA) conducted to characterize the foam has shown it to be stable at temperatures exceeding 550 degrees Celsius [5]. These CFF material properties have the potential to improve upon current ballistic protection materials by decreasing weight and improving shock absorption while remaining mechanically and thermally stable.

### **D. EARLIER RESEARCH EFFORTS**

Efforts to generate three-dimensional structures using CFF material as a primary structural component have been attempted with varying levels of success. One such method created composites, formed from a combination of polymers and carbon nanoparticles [2]. The purpose was to create a material for use as a strain gauge. The composite structures had the desired electrical conductivity gained from the carbon nanoparticles. The composite structure also gained unwanted qualities from the polymers, such as increased density, and low thermal stability [6–8]. Several methods have used capillary forces, caused by the drying of a liquid between two structures, to cause the predictable formation of patterns with in strait nanotube arrays [6, 9]. Of the structures that have been created using the post CFF production method, none were found to be successful thus far in creating a mechanically robust foam structure. The process found

most successful in the creation of CFFs use the constrained formation of fibrous nanostructures process (CoFFiN) [10].

## **E. THESIS OUTLINE**

This project is composed of both an experimental approach to generate the carbon nanofiber foam mat of 5 x 5 x 0.5 inches and a simulation that aids the understanding of how the gases used during the CFF growth are distributed within the mold used to generate it. The thesis is divided into four chapters, the present one introducing the subject, followed by experimental methods, results and discussion, and conclusion chapters. The experimental methods chapter will provide details into the experimental equipment and precursors used as well as the individual experimental setup and conditions to scale up the growth experiments. The results analysis chapter will provide a detailed discussion of the CFF generation process variables, the overall chemical vapor deposition (CVD) foam generation mechanism, foam characterization, as well as a summary of the variables conditions required for successful foam scalability. The conclusion chapter summarizes all the milestones achieved.

### **1. Objectives**

The primary objective for this thesis is to create a chamber capable of containing CFF environmental conditions that is able support the foam generation. This objective will be affirmed by producing a homogenous, mechanically robust, interconnected throughout CFF sample large enough for potential testing as part of a ballistics target system.

### **2. Hypotheses**

We can scale the production of CFF and manufacture homogenous, interconnected, and mechanically robust foam samples through the use of a modified CVD process.

The variables believed to be most important to the scalability are time and flow. The CVD process variables will be controlled and employed inside a growth chamber. This chamber will constrain the growth of fibers in order to generate a CFF mat. If

successful, the mat will fill the entirety of the chamber while maintaining its mechanical robustness.

### **3. Tasks**

The tasks determined necessary to investigate the thesis hypothesis are:

- Design and manufacture a CFF chamber capable of directing gas flows through the system and capable of withstanding the moderate temperatures required for the CFF generation process.
- Generate a homogenous, interwoven CFF mat from a catalyst in a carbon rich environment to validate the scaled up CFF chamber design and support proof of concept.
- Conduct characterization of CFF results to ensure continuity of physical features.
- Analyze experimental results and determine variable impacts. Identify variables critical to scaled production of CFF.
- Identify areas where costs can be reduced or cost can be recuperated.

### **4. Contributions of This Work**

CFF materials have been found to have remarkable mechanical and electrical characteristics [5, 11–13]. Successful attempts to generate these CFF materials have produced small samples capable of supporting characterization techniques and mechanical and electrical testing. This work expands on earlier research by increasing the manufacturing capability of CFF materials, which will allow for more complex physical testing [5]. It will also identify the critical variables that control its scalability.

## **II. EXPERIMENTAL METHODS**

The main objectives of this thesis were to determine the potential scalability of producing carbon nanofibers into larger foams and whether these foams will possess the same desired physical properties observed in previously studied smaller specimens. The process selected to grow the CFF was the CoFFiN method. This process has been successful in creating small CFF samples and involves growing CFF in a constrained space using a catalyst in an oxygen/ethylene environment [5]. Constraining the growth of the CFF within the confined chamber is important because it forces the growing fibers to become a single tangled interwoven mat. The experimental method chapter will discuss the specifics of the dimensions and rationale for the mold design to grow carbon nanofiber foam structures. It will also cover the CFF precursor materials used and the manufacturing process description.

### **A. MOLD DESIGN**

The generation of a large CFF required the creation of a new mold chamber. The new chamber had to be at least 5 x 4 x 1 inches in order to create samples that meet the requirements for shock wave and ballistic testing. It was also reasoned that this increase in size was enough to represent meaningful scalability. Stainless steel was chosen as the design material because it provided good thermal resistance to support the CFF growth process. It also has acceptable corrosion protection while mechanically withstanding the temperatures needed for the growth process. Other materials considered for the chamber design were aluminum, ceramic oxides and tungsten. Aluminum was discarded as an appropriate material choice due its melting points (660.32 degrees Celsius) proximity to our CFF growth temperature (550 degrees Celsius). A ceramic mold was ruled out because of the likelihood of complications arising with controlling the hermetic environment and due to its brittleness. Tungsten and other metals were discarded as options due to their higher purchase price.

The finalized chamber design shown in Figure 1 contains two gas flow inlets at one end. These inlets open into a small inlet chamber. The inlet chamber provides the

gases additional space to diffuse thoroughly and create a homogenous mixture prior to reaching the catalyst within main chamber. The inlet chamber is connected to the main chamber by seven small 1/8th inch connecting tunnels. These tunnels are evenly spaced along the length of the wall separating the main chamber from the inlet chamber. The gases pass through the small tunnels then flow into the main chamber. Once the gases pass to the far end of the main chamber, they reach another separating wall with a similar set of seven evenly spaced small connecting tunnels. These tubes pass into another separate outlet chamber. The outlet chamber has two openings that allow the exhaust gases to exit the mold.

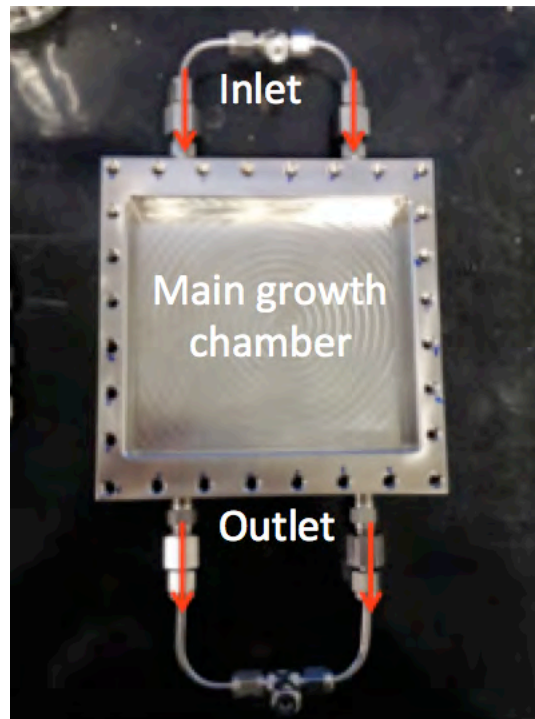


Figure 1. CFF mold chamber with attached inlet and outlet connections.

A 6 x 6 x 2-inch block of stainless steel was milled into the finalized design using a Hass VF-6 CNC mill capable of 5-axis rotation due to the use of its TRT-310 trunnion table (shown in Figure 2). The CNC machine was used to create all threaded connections, the gas flow inlets and outlets, the inlet and outlet chambers, and the larger main chamber. The gas flow tunnels that connect the chambers were created using a drill press.

These chambers and tunnels are identified in Figure 3. The external access holes (which were required to create the chambers and tunnels) were completely sealed by plugging the hole with 308 stainless steel welding filler material.

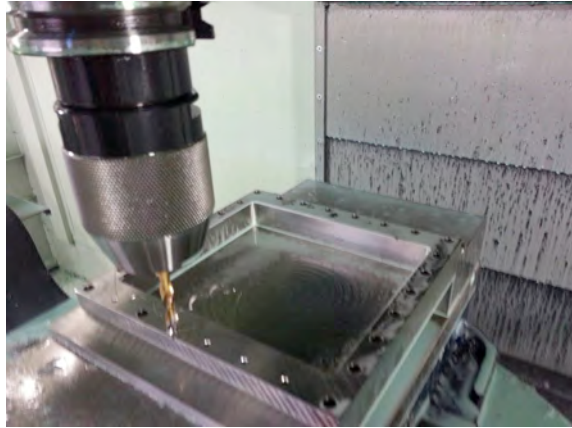


Figure 2. CNC machine creating the main CFF growth chamber.

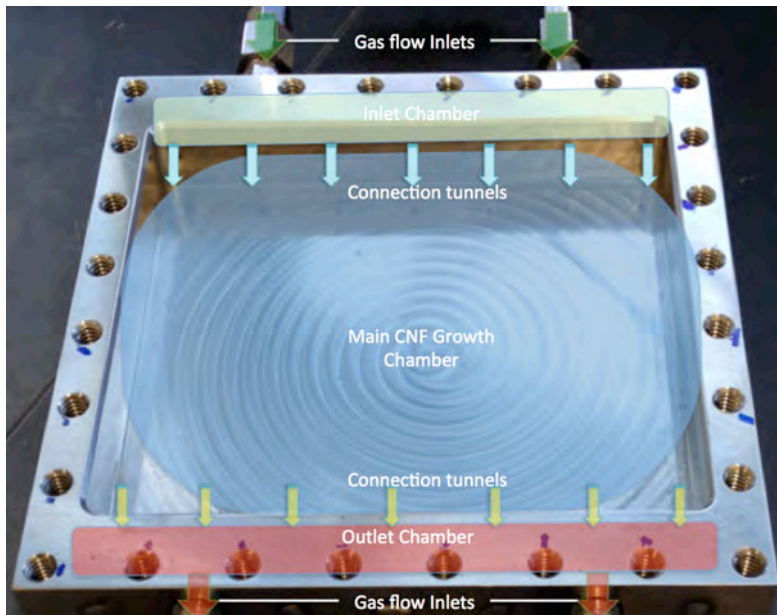


Figure 3. Finalized chamber for CFF growth. The figure shows the path traveled by the gases through the mold.

A lid made of the same stainless steel was used to close the mold. The lid had a small 0.05 inch beveled section that allowed for it to fit exactly within the main chamber. The lid was screwed to the mold using 28 stainless steel bolts, providing a hermetic seal.

Both mold inlet and outlet connections were created using Swagelok brand 1/4th inch fittings. The fittings were arranged to enable the connection and disconnection of 1/8 inch stainless steel tubing. These tubes allow for the transportation of gases to and from the mold within the high temperatures of the furnace without the risk of damage caused by the high temperatures generated within the furnace. The stainless inlet tube was made longer than the exit tube. The inlet tube curves back and forth in order to fit within the confines of the furnace. The additional length also provides additional residence time for the transported gases to come to the desired experimental temperature prior to reaching the catalyst within the main chamber.

SOLIDWORKS computer-aided design software was used to create computer models that were then used by ANSYS CFX fluid modeling software to model flows within the chamber [14]. The ANSYS CFX software was used to provide a better understanding of how the precursor gases would travel through the interior of the chamber [15]. ANSYS was also employed to validate the gas direction when using stainless steel deflector SIX, as explained in Chapter III. The assumptions made for the computer model were that the precursor gases were ideal and that the flow is laminar.

## **B. CARBON NANOFIBER PRODUCTION**

### **1. Experimental Setup Procedures**

The experimental setup procedures for the CFF generation can be broken into three categories: cleanliness/lubrication, setup/palladium placement and gas mixtures.

#### ***a. Cleanliness/Lubrication***

Each of the individually performed experiments followed the same essential setup steps necessary to conduct the CFF growth properly. Cleanliness was extremely important due to the recycled CFF chamber components through all of the experiments. The CFF growth chamber, chamber lid, and deflectors were first carefully cleaned using a soft bristled brush and Ethanol Alcohol. The cleaned chamber components were then dried using compressed air. The bolts that were used to secure the lid into place were sonicated in a fresh water bath for (5) minutes to remove lubricants. The bolts were then

dried using standard household paper towels. After being thoroughly dried, a thin film of VersaChem anti-seize thread lubricant (type-13 high temperature copper formula) was applied to each bolt's threads.

***b. Setup/Palladium Placement***

The Palladium ((Pd) powder <1  $\mu\text{m}$ , purity >99.9% trace metals basis) catalyst was measured using an Ohaus, Explorer Pro scale. The Palladium powder was distributed by hand within the main chamber using a thin strip of stainless steel. The powder was spread into small diagonal columns approximately 1/8th inch thick (with respect to the forward wall) within the CFF growth chamber. This was done in an effort to distribute the catalyst evenly throughout the entirety of the chamber in a manner that would be easily repeatable for all experiments. Figure 4 shows this distribution within the main chamber.

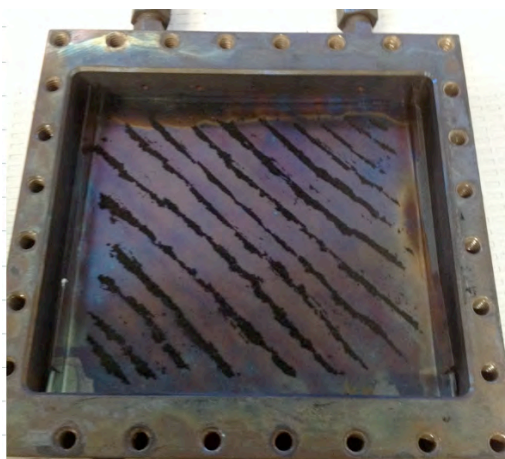


Figure 4. Palladium arrangement (0.5 gram) within the main mold chamber.

The experiment's deflector (when used) was put into place followed by the CFF growth chamber lid. The lid was secured with the recently lubricated bolts in a star pattern to create a hermetic seal between the chamber rim and lid. Stainless steel gas flow tubes of 1/8th inch diameter were then attached to the in/out flow gas diffusion chamber connections. The assembled CFF chamber components were then carefully placed inside a Thermo Scientific; LindBerg Blue M model BF51442C furnace shown in Figure 5 and

Figure 6. The gas flow tubes were navigated through the furnaces 1/2-inch by 2-inch window and the furnace door was closed. The furnace's window was then sealed using a non-heat conductive packing material.



Figure 5. Lindberg Blue M model BF51442C furnace shown from the front with chamber door closed and window packing material in place.



Figure 6. Interior chamber shown with the door open from the front.

A MKS mass flow controller (model MKS 647a), shown in Figure 7. was connected to the inlet 1/8th inch stainless steel gas tube via a Swagelok connection using via a 1/4th inch polyurethane gas tube. The outlet 1/8th inch stainless steel gas tube was

connected to a separate 1/4th inch polyurethane tube. This tube vented exhaust gases and water vapor into an erlenmeyer flask with a water reservoir containing a side exit creating an exhaust trap. This exhaust trap is shown in Figure 8. The exhaust gases then passed through the side exit into another erlenmeyer containing zeolite and permanganate to dilute the exhaust gases and trap unreacted ethylene prior to their release.



Figure 7. MKS mass flow controller (model MKS 647a).



Figure 8. Erlenmeyer exhaust trap utilizing zeolite and permanganate.

**c. Gas Mixture**

A flow of pure compressed nitrogen gas of ultra high purity (UPH) running at 300 SCCM was used to remove the air from the system. This created an inert environment from which to proceed with the experiment. The environment also prevented accidental oxidation of the palladium catalyst, which could become likely as the temperature within the system increased due to the rising furnace temperatures. The gas flowing into the system was controlled using the MKS mass flow controller. The nitrogen ran for 15 minutes to allow the purging of the lines and chambers within the mold. After the nitrogen environment had been established, the furnace was switched on and set to 550 degrees Celsius. Once the desired temperature was reached, ethylene (99.90%) and oxygen were added to the inlet flow of the system. The ethylene flow started at a rate of 45 SCCM. The oxygen was started at 5 SCCM and increased every 2 minutes by 5 SCCM until a flow of 45 SCCM was reached. This was done as a precautionary measure to prevent creating an exothermic reaction by adding too much oxygen to a heated fuel source. Gas exit flows were monitored using an external gas flow meter to monitor for any blockages within the mold.

**C. DESIGN SCALE UP**

**1. Preliminary CFF Experiments**

The experimental process used for this thesis follows the same protocols of previous experimental studies conducted for the creation of carbon nanofibers [5, 16]. These successful preliminary experimental procedures were then modified to replicate the results within the newly designed larger mold chamber. The preliminary experimental methods are briefly reviewed below to aid in explaining the decisions made for this thesis. The first experiments conducted utilized a stainless steel mold with a single cavity of 0.35 x 1 x 2.35 inches. That mold had orifices at its two ends to allow for the connection of both the inlet and exhaust tubes. Palladium powder (0.02 grams) was spread the length of the chamber as shown in Figure 9. After sealing the chamber with a lid, the mold was placed inside a Lindberg Blue Mini-Mite furnace with area dimensions of 14 x 7.75 x 5.5 inches. The inlet was fed a gas mixture of nitrogen, oxygen and

ethylene using the MKS mass flow controller. Nitrogen flushed the system at a rate of 100 SCCM for 10 minutes to create the base nitrogen environment from which the experiment was started. The furnace was started and set to 550 degrees Celsius. Once the furnace reached its desired operating temperature, oxygen and ethylene were added to the flow. The ethylene was started at 15 SCCM. The oxygen was started at 10 SCCM and increased to 15 SCCM after 5 minutes. These conditions were kept for 3 hours. After the 3-hour period, the furnace was switched off and the ethylene and oxygen flows were secured and the nitrogen flow reduced to 30 SCCM for 10 minutes. Following the 10-minute period, the nitrogen was secured and the mold sat until cool.



Figure 9. Early CFF experimental mold (dimensions of 0.5 x 0.344 x 2.25 inches) shown with 0.02 grams of palladium distributed within the chamber.

## 2. **Modification of Scale Up Experiment Variables to Produce Larger Mat**

Scale up of the production process from the preliminary proof of process experiments required the selection of variables that we would modify or hold constant from earlier preliminary CFF experiments.

### *a. Palladium*

The increase in the amount of palladium catalyst used from the preliminary CFF experiments was scaled based on the increased area between the two experimental chambers. The chamber floor within the preliminary mold was 1.125 in<sup>2</sup> while that of the scaled chamber floor is 20 in<sup>2</sup>. It was expected that this 17.77 times increase in the area required a similar increase in the amount of the palladium catalyst used. Increasing the palladium correspondingly justified the use of 0.5 grams for all of the scale up experiments.

***b. Gas flow***

The increased palladium use in the scaled up experiment drove the need to increase the amount of ethylene and oxygen. Both gases are needed in order to create an environment suitable for the generation of the CFF. Both the Preliminary and scaled up CFF experimental flow rates are presented below in Table 1. Ethylene and oxygen flow rates of 45 SCCM was determined to be sufficient to provide the environmental conditions necessary for catalyst generation of CFF.

Table 1. Experimental gas flows used for experiments.

Experiment	Gases (SCCM)		
	N2	O2	Ethylene
Preliminary Experiments	100	15	15
Large Mold Experiments	300	45	45

***c. Temperature***

The temperature was to remain at 550 degrees Celsius. This is due to previous studies that showed growth of CFF was greatest when this temperature was maintained [5, 12, 13]. A discussion of the temperature, gas and radical creation are explained in detail in Chapter III. Since the gas flow velocity will increase in the scaled up experiments due to increased fluid flow through similar sized tubes, a way to ensure the temperature of the gases reached their optimal temperature prior to arriving at the main chamber needed to be developed. To ensure that the higher gas flow rates reached the desired temperature of 550 degrees, the inlet piping into the scaled mold required modification. To increase the gases residence time within the furnace, the inlet 1/8th inch pipe's length was increased and several "S" type curves were formed to allow the increased length to fit within the furnace dimensions and is shown in Figure 10.



Figure 10. Increased chamber inlet length shown attached to the scaled mold.

### 3. Utilization of Gas Flow Deflectors

The gas flow distribution path was simulated using ANSYS software [15]. The resulting model showed precursor gas flow paths that would reach all regions of the interior chamber. As shown in Figure 11 the flow velocities were highest at the inlets and outlets of the designed chamber. The velocities were significantly reduced prior to reaching the main CFF growth chamber thru the use of the inlet chamber.

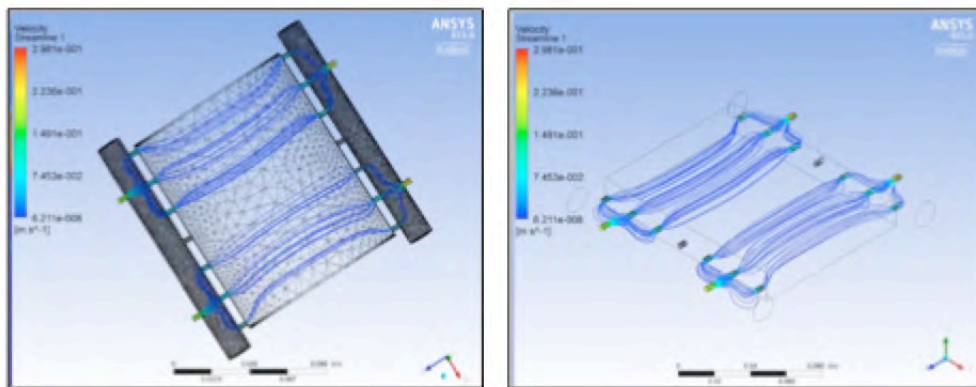


Figure 11. ANSYS modeling of the mold chamber shows the flow velocities along within the chamber.

Due to the physical restraints placed on the mold design by the dimensions of the furnace available, the gases had to travel in a path that ran lengthwise through the main chamber. This caused the entry region to receive continuous gas flows while the palladium in the rear chamber areas was not being reached by the same gas flow. In the effort to mitigate this problem and control the adequate flow distribution required for foam generation, a series of deflectors were created to control the distribution of gas to all regions of the main chamber and promote fiber growth throughout the chamber. Stainless steel was again chosen as the material for the deflector design. In total, seven deflector variations were utilized in the experiments.

**a. Rod Deflector ONE**

The first deflector design, shown in Figure 12. utilized within the main chamber, was created from a 1/8-inch diameter stainless steel rod. The rod was bent with hand tools to form a cylindrical barrier and was placed in front of the main chamber gas flow inlets. The deflector has a single small bend at its base that kept the deflector in an upright position within the mold as the experiment was run. The purpose of the deflector was to increase the flows turbulence within the chamber as the gases passed through the cylinder.



Figure 12. Image showing the length of Deflector ONE.

**b. Foil Deflector ONE**

The next deflector design in the series utilized a single piece of stainless steel shim (Trinity Brand Industries, Inc., Part No. 6316-4) that ran the length of the main chamber inlets and is shown in Figure 13. The designs that follow are modifications of this deflector. This material was chosen to create all follow-on deflectors because its

material closely matched the mold material and thus had matching material properties. It also proved to be an easy material base to create the desired deflector shapes. This early deflector design forced the gas flow through open gaps left above and below the inlets.

A chamber base was also added to the deflector design to help assist with the removal of CFF and to prevent damage to the foam and chamber as the foam was removed from the mold. The base had two forward walls that ran half the length of the chamber and parallel to the sidewalls of the main chamber. The rear of the deflector chamber base had two prongs that touched the rear sidewalls at the rear of the chamber to ensure the base and deflector's position both remained constant within the mold as the experiment ran. This chamber base was used in all follow-on foil deflector experiments.



Figure 13. Image showing foil deflector base in position within the chamber.

*c. Foil Deflector TWO*

The second foil deflector design, shown in Figure 14. was modified from the first and replaced the upper gap with a cover that ran nearly the entire length of the main chamber. A gap was created in the rear of the covered section to distribute gas flows to reach the rear and center sections of the main chamber.

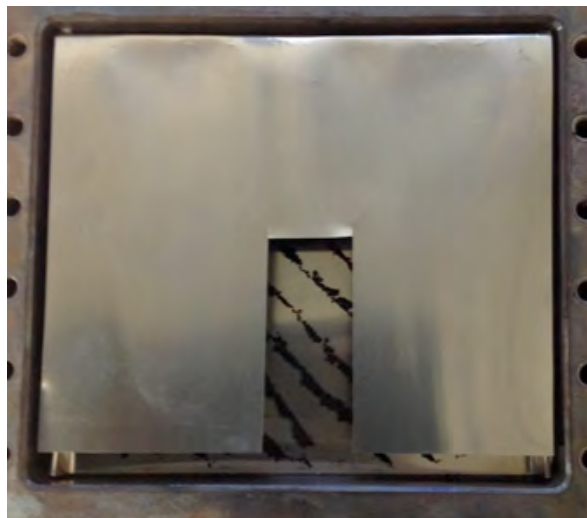


Figure 14. Foil Deflector TWO in position within the chamber.

*d. Foil Deflector THREE*

The third deflector, shown in Figure 15. increased the gas flow reaching the center of the chamber through the addition of a nearly  $\frac{1}{2}$ -inch slit in the cover. It is worth noting that a gap of a couple of mm existed between this cover and the lid of the chamber, allowing gases to reach the catalyst particles located on the base.

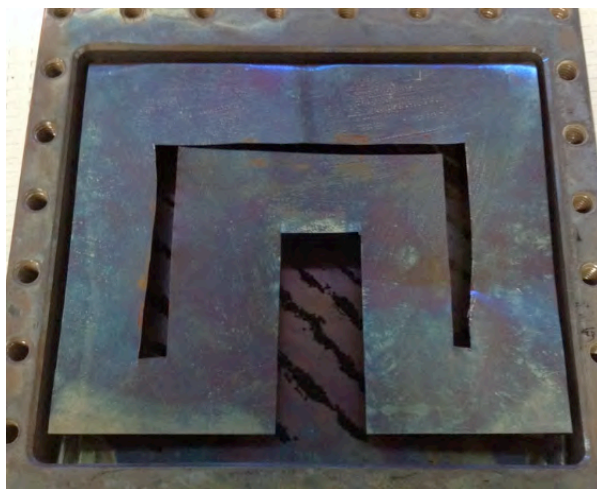


Figure 15. Foil Deflector THREE in position within the chamber.

*e. Foil Deflector FOUR*

Deflector four, shown in Figure 16. decreased the area and gas flow available to the rear center section of the main chamber by replacing the 1 x 2-inch rectangular center cut out with (2) ½-inch slits similar to the ones added in deflector three. This deflector also increased the lower forward gap that has been unchanged since Foil Deflector ONE.

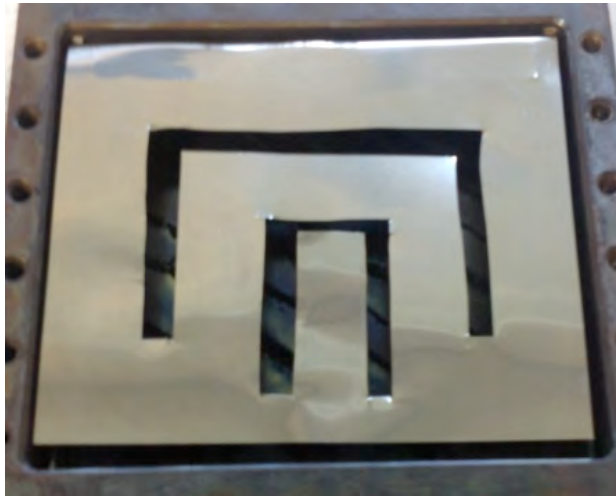


Figure 16. Foil Deflector FOUR in position within the chamber.

*f. Foil Deflector FIVE*

Deflector five, shown in Figure 17. returned to the lower forward gap dimensions used in Foil Deflector ONE. It also further decreased the flow to the rear center chamber by utilizing two single parallel slits 1/4 inch wide. Attaching a cover over the rear section of deflector three made these changes.



Figure 17. Foil Deflector FIVE in position within the chamber.

***g. Foil Deflector SIX***

Deflector six added a small section of stainless steel foil to the rear of deflector five to prevent the CFF growth from blocking and clogging the gas outlets in the rear of the chamber. The strip was made to seat as close as possible to the chamber floor and provided a narrow gap that sat below the deflector cover. The strip, shown in Figure 18, was held in position by the chamber floor prongs that sit at the rear of the chamber. This provided ample gas exhaust while constraining the growth to the main chamber area.

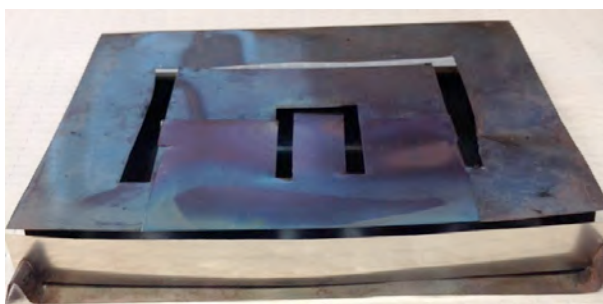


Figure 18. Foil Deflector SIX in position within the chamber.

#### **D. CATALYST RECOVERY**

The significant cost of purchasing the palladium catalyst for the production of CFF represents a limitation for the use of the process just described unless the catalyst can be recovered and recycled. The cost of a single gram of the palladium catalyst is \$250.00. This creates a desire to find ways to reduce the amount of palladium required to grow the foam or recover the spent catalyst that remains behind within the foam after the combustion process. Novel approaches aimed at recovering spent palladium catalyst used in other processes have been conducted by Sarioglan [17] Barakat et al. [18], and Jasra et al. [19], demonstrating potential methods that may be successful at removing and recovering the valuable palladium without damaging the newly created materials and are discussed in further detail in Chapter III. To demonstrate the ability to extract the palladium from the CFF, an experiment was devised using the Sarioglan recovery method referenced. The experiment sought to remove palladium via a leaching reaction using an acidic solution and a moderate temperature. Two different solutions were created to compare the amount of palladium recovered from foam samples. The first solution (solution 1) was an aqueous solution composed of 10% hydrochloric acid. The second solution (solution 2) was an aqueous solution composed of 10% hydrochloric acid and 5% hydrogen peroxide. Each solution was measured, and placed into separate clear Pyrex measuring containers. Using a Corning PC-220 hot plate, the solutions were brought to a temperature of 60 degrees Celsius. Two samples were cut from Foil Deflector ONE's CFF experiment. Each sample was taken from good foam created in the forward region of the main mold chamber. The samples were cut into similar sized cylindrical shapes using a razor. The samples were then weighed and measurements were recorded. When the solutions reached the desired temperature, each sample was placed within a solution container and was held submerged using silica glass. The samples remained submerged at a constant temperature for 90 minutes then were removed from the solution. The samples were then placed into the CFF main mold chamber and the chamber sealed. The mold was placed inside the furnace and connected to the MKS mass flow controller. Nitrogen was run through the mold at 100 SCCM to provide a nonreactive environment. The furnace dried at 550 degrees for 3 hours. Upon removal from the chamber, the samples

were cut so that a cross-sectional area of the center and outer surface were viewable. These sample cuts were attached to the SEM sample pedestals using a conductive liquid silver solution then placed into a vacuum of 30 PSI.

## **E. CHARACTERIZATION METHODS**

### **1. Scanning Electron Microscopy (SEM) and Back-Scattered Electron Signal (BSE)**

Carbon Nano-Fiber SEM and BSE characterization were completed using a Zeiss Neon 40 electron microscope, shown in Figure 19. Images taken at 1k, 5k and 15k times magnification utilized extra high tension (EHT) of 20 kV and were taken using a working distance between 5~10 mm.

Samples were taken from each of the completed CFF experiments for comparison. Comparison samples were taken from forward regions near inlet, where the foam produced was of desired production quality. Sample specimens were attached to individual pedestals using a conductive liquid silver solution and were placed in a vacuum of 30 PSI.

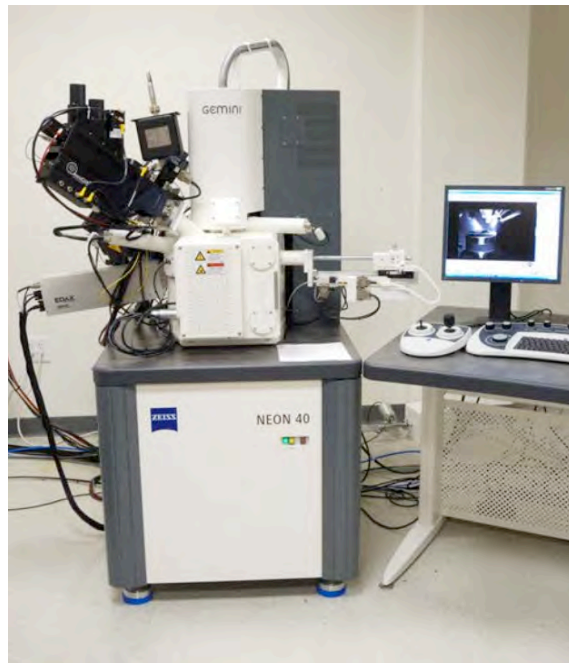


Figure 19. Zeiss Neon 40 electron microscope.

## 2. Brunauer-Emmett-Teller (BET) Characterization

BET analysis of the fibers surface area was conducted using a Nova 4200e Surface area and Pore Size Analyzer, shown in Figure 20. The results were obtained using nitrogen as the systems working adsorbent. The results were displayed using Nova software.

Each sample was cut, weighed and then placed into a thin glass tube cell. Each sample's surface cleaning was conducted using a degassing procedure. Samples in their cells were placed the Nova 4200e and were heated to 100 degrees Celsius for 30 minutes before raising the temperature to 200 degrees for an additional 120 minutes. After the degassing process, the cells were placed in a liquid nitrogen bath and small amounts of nitrogen were allowed to adsorb onto the sample surface so that an accurate calculation of the surface area could be determined.



Figure 20. Nova 4200e.

THIS PAGE INTENTIONALLY LEFT BLANK

### III. RESULTS AND DISCUSSION

The results obtained from the experiments showed a steady progression toward the ultimate goal of modifying variable conditions to create a single, solid, interwoven mat of CFF. Conditions were selected based on results from earlier CFF research and then tailored to meet the scalability desired for this body of work. This chapter will begin with a discussion of the principles of fiber growth followed by the experiment results and analysis. The results of this thesis are summarized below in the order that the experiments were carried out.

#### A. FIBER GROWTH

In order to understand the challenges faced to scale up the production of the carbon nanofiber foams, central task of this thesis, a few basic concepts need to be reviewed regarding the structure and conditions of growth during the fabrication process:

The element carbon can be found as diverse allotropic forms, each with a different structure, some of the most common are diamond, graphite, fullerenes and carbon nanotubes (CNT). The structural differences between those can be related to the way that carbon bonds, since this element can be linked to 2, 3 or 4 other atoms due to its electronic configuration,  $1s^2 2s^2 2p^2$ . In order to equalize the energy differences between the orbitals the 4 electrons in the outer shell can combine to form 3 types of hybrids. The  $sp^3$  orbitals acquire a tetragonal arrangement, that is, form a tridimensional structure like the ones found in diamond or  $CH_4$  (methane). The  $sp^2$  orbitals are trigonal and planar and are typical of graphite and  $H_2C=CH_2$  (ethylene). The  $sp^1$  orbitals are linear and found in  $HC\equiv CH$  (acetylene) [20].

Graphite consists of separated layers of carbon atoms that are  $sp^2$  hybridized. Such structure has electrons (one for each carbon atom) that form a  $\pi$ -electron system, that is, a charge cloud that is shared by all carbon atoms. In graphite that cloud exists in both sides of the layered structure, with no primary bonds in between layers, the only force keeping them together being a Van der Waals interaction. The layers in the structure can easily slide one past another.

Carbon nanotubes share the properties described above for graphite, since they can be described as a rolled up single sheet of graphite, also named Single-wall carbon nanotube (SWCNT). When more than a tube is nested in others in a concentric arrangement we called them Multi-wall carbon nanotubes (MWCNT). The diameter of CNT is in the order of 0.4 nm to a few nm, however, their length can reach mm [10, 21].

In this thesis, the materials generated are referred as Carbon nanofibers foam (CFF) and it is worth mentioning that despite having, in many cases, the same diameters that MWCNT present, they do not share the same structure. The former are cylindrical structures with no empty space inside (they are fiber based), while the MWCNT present always a tubular structure to differentiate them from the so-called carbon nanofoams.

The name carbon nanofoam has been given to a magnetic carbon substance made by focusing a laser ablation system into graphite in a chamber filled with argon gas. During such process, the high temperatures achieved (18,000 C) by the system evaporate the graphite into single carbon atoms that later condenses into clusters as the vapor is cooled. The large-scale structure of a carbon nanofoam is composed of  $sp^2$  and  $sp^3$  bonded carbon atoms, has ferromagnetic behavior and is extremely lightweight [22] (See Figure 21).

In contrast, the foams described herein, previously introduced by our team [16], are made up by bundles of carbon nanofibers, also known as vapor grown carbon fibers. The vapor growth process is described with more detail in the next paragraphs. The nanofibers present diameters in the range of a few nm to about 300 nm and intertwine among themselves (see Figure 21) forming a highly porous arrangement which tridimensional form resembles foam.

The word foam has been traditionally used to describe a substance that is made by trapping pockets of gas in a liquid or solid and neither the nanofoams nor the nanofiber foams structures just described adjust to such definition. An example of a polymeric polyurethane foam structure from Pierson [20] is presented in Figure 21.

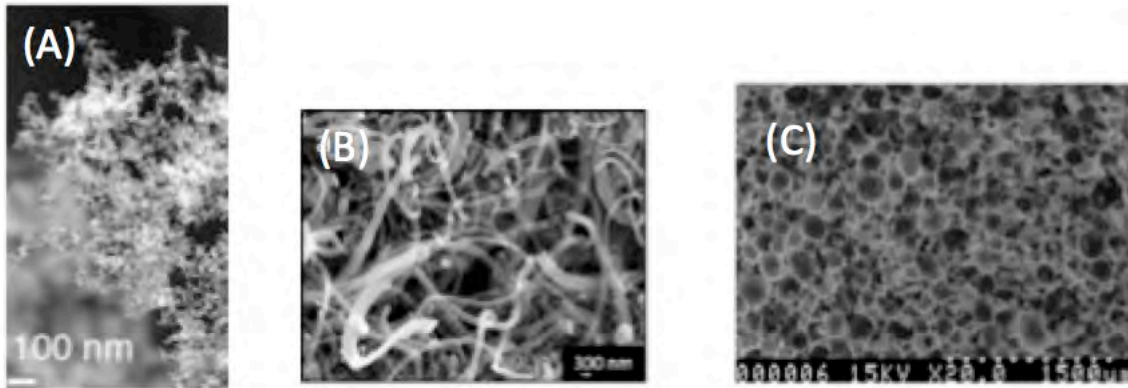


Figure 21. The carbon nanofoam shown in image a, has carbon structures ranging from 1–10 nm in diameter. These structures appear to be assembled in a highly chaotic and unorganized formation. The carbon nanofibers shown in image b have structures ranging from 100 - 300 nm in diameter. The individual fibers shown in this image all have the typical symmetric cylindrical appearance. The carbon structure shown in image c on the other hand is the largest of the three image structures. The diameters of these structures are measured in microns which is several orders of magnitude larger than the structures seen in image a and b, from [16, 20, 22]

## B. CONSTRAINED FORMATION OF FIBROUS NANOSTRUCTURES

The constrained formation of fibrous nanostructures (CoFFiN) process used in the generation of CFF is a modification of the chemical vapor deposition (CVD) process. CVD typically uses a low temperature [500-1200° C] thermal decomposition of a carbon rich vapor to create carbon structures. This low temperature thermal decomposition, also called catalytic pyrolysis, is achieved by using a metal catalyst [8]. This process starts when a hydrocarbon rich gas is passed to a heated vessel that contains a catalyst. This vessel must be kept at a sufficiently high temperature to allow for the thermal decomposition of the gas into a nanostructure by the catalyst. The CVD variables that impact the gas decomposition, which ultimately facilitates the growth of CFF nanostructures, are the gas precursors, gas flows, choice of catalyst, and temperature. The primary difference between the CoFFiN and CVD method is that CVD does not constrain the area available for the growth of the carbon structures. CVD allows the chemical reaction to dominate the physical form of the carbon nanostructure product being generated. The CoFFiN method, on the other hand, restricts the area available for the growth of nanostructures. This is significant because limiting the growth region creates

an additional substantial variable through which we can improve the characteristics of the CFF products being generated. The addition of the growth restriction has a direct impact on the gas decomposition because it impacts the CVD variables specifically the gas flow.

### **1. Precursors Gases**

Precursors control the morphology of the CFF structure materials being generated. This physical impact to the structures is caused by the thermal breakdown of the molecular structure of the gas. For example, methane's molecular structure generally produces straight CNTs while fullerene's molecular structure produces curved CNT's [23, 24]. The most highly used carbon precursors for CVD are acetylene, benzene, carbon monoxide, cyclohexane, and fullerene, ethanol, ethylene, and methane [8]. In some cases, oxygen is added to the precursor mixture. This is occasionally due to a catalyst's oxide being able to create greater catalytic activity than the pure catalyst alone [25].

### **2. Catalysts**

The most common CVD catalysts have two basic qualities that make them preferable for use. First, a high capacity to dissolve carbon at high temperature allows the catalyst to extract a greater amount of carbon from the precursor. Second, a high carbon diffusion rate allows the efficient formation of the carbon structure. The commonly used catalysts for generation of CFF's are Ag, Au, Co, Cu, Fe, Ni, Pd., and Pt. [8]. Catalysts play an important role in the enablement of the hydrocarbon decomposition as well as the physical size of the CFF materials being generated. Catalyst particle sizes typically are required to be on the nanometer scale to allow for the precursors low temperature decomposition. Another important role the catalyst serves during the growth of carbon nanostructures is preventing formation of a carbon cap, which can form due to dangling carbon bonds. The formation of the cap prevents the catalysts decomposition of the hydrocarbon gas. This formation ultimately ceases the growth process by encapsulating the catalyst in the structure and precludes the further growth. The catalyst's adhesion to the nanostructure's dangling carbon bonds must be greater than the energy gained from the formation of the carbon cap to prevent this formation. Co, Fe and Ni, and are well suited for use in the formation of CNT's due to their high catalyst adhesion. Au, Co, Cu,

and Pd all have weaker adhesion properties. This makes them better suited for the formation of carbon nanofibers [26].

### **3. Temperature**

Temperature impacts the CFF structure material's rate of growth in the CVD process. This rate of growth is also highly dependent on the choice of catalyst used in the process. Previous research conducted using Pd as a catalyst with an ethylene precursor showed that highest growth rates were achieved using ~550°C [5].

### **C. GROWTH MODEL THEORY**

The vapor-liquid-solid (VLS) growth model offers the best theory for the actual physical mechanics for the growth of carbon nanostructures from a catalyst and hydrocarbon gas mixture [8, 27]. When the hydrocarbon gas arrives at the heated catalyst nanoparticle, the gas decomposes into both carbon and hydrogen species due to a chemical reaction. The carbon is absorbed into the catalyst while the hydrogen remains behind as exhaust vapor. Once the catalyst nanoparticle reaches its carbon solubility limit, a three-phase state is reached, where a solid; liquid and gas are all present within the catalyst's activity [28]. The carbon precipitates out of the catalyst and crystallizes, forming the base of the CFF nanostructure material. The direction of the carbon growth will be determined by the interaction of the catalyst and the substrate. The catalyst's interaction with its substrate will determine the direction of the carbon growth [29]. If the interaction is weak and an acute contact angle is formed between the catalyst and the substrate, the carbon will precipitate at the catalyst's bottom and force the catalyst to lift off the substrate, this is called the "tip growth" model [8]. If there is a strong interaction between the catalyst and the substrate and an obtuse contact angle is formed, the carbon will precipitate farthest from the substrate and the CFF structure will form out the top of the catalyst, this process is called the "base growth" model [8]. This process will continue so long as the conditions for hydrocarbon decomposition remain achievable. Figure 22 shows the growth mechanics explained in detail above.

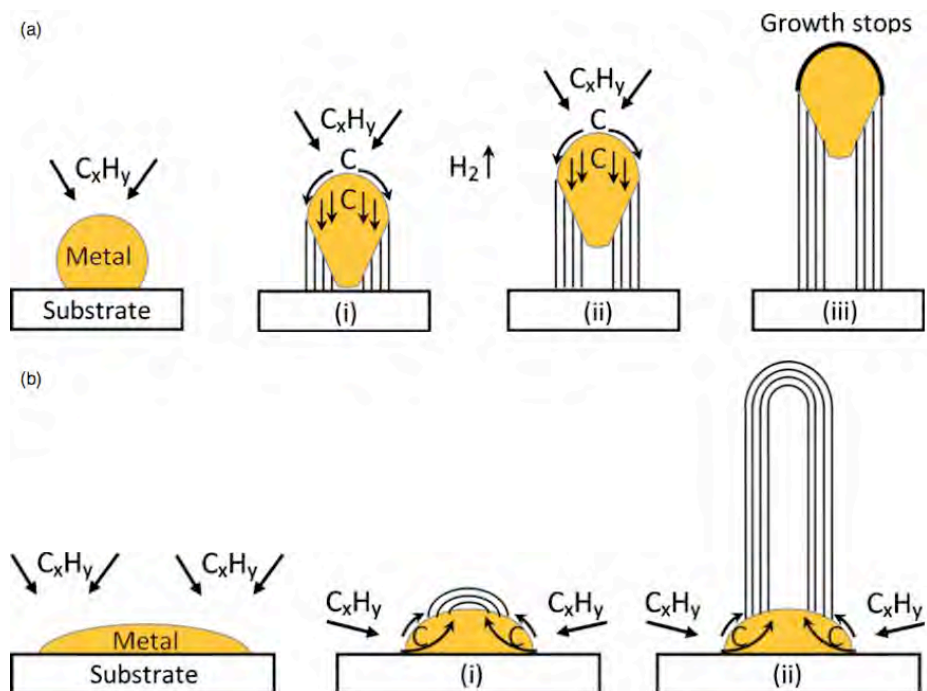


Figure 22. Depictions of the “tip-growth” (a) and “base growth” (b) models showing the vapor-liquid-solid growth process, from [8].

#### D. CATALYST RECOVERY DISCUSSION

The value of the metal catalysts used in the CFF production process requires the development of a method that is capable of recovering and reusing the spent catalyst without damaging the newly created CFF material. Since CFF generation requires the use of catalysts, such a process is economically desirable. Incineration is a method that is typically used to recover metal catalysts but this technique oxidizes palladium, thus requiring further reduction steps [17]. Sarioglan states that two hydrometallurgical methods have been used for the recovery of palladium-spent catalyst [17]. The first technique dissolves the suspending material containing the palladium-spent catalyst using chemical reagents. This method would not be suitable as a recovery method for CFF production since it would destroy the CFF material. The second method is a leaching method, which dissolves the palladium rather than the suspending material by using a hydrochloric acid solution or acidic oxidant solutions composed of chloride salts and nitric acid [17]. The palladium is then dissolved and then separated from the solution by

reduction [18]. This second method leaves the suspending structure intact, which makes its potential use as a catalyst recovery method for CFF promising.

## **E. FOAM ANALYSIS**

### **1. Preliminary CFF Experiment**

Several early CFF experiments conducted utilizing the smaller CFF growth chamber were conducted to demonstrate an ability to create CFF of desirable quality. The foam created using the palladium catalyst appeared consistent throughout the mold chamber as shown in Figure 23. The mold chamber was completely filled with foam. The foam was dense yet flexible and did not crumble under when mildly compressed under the pressure applied via a spatula. Figure 24. shows that the foam could be removed mostly intact. Unfortunately tearing occurred where the foam had adhered to the surface of the chamber walls, which made it necessary to scrape the chamber walls to remove the remaining foam fragments.



Figure 23. Preliminary CFF Experiment prior to its removal from the chamber.



Figure 24. Image of foam after removal from the chamber.

The foam was then characterized using the Zeiss SEM. Images revealed the diameter sizes of the fibers generated during the experiment and are seen in Figure 26. The SEM images were then analyzed using the image analysis software Image-J [30]. A

diameter size distribution was generated in order to create a reference that would be used to compare the scaled experiment foam results against. The diameter size distributions are plotted in Figure 25. The fiber diameters were found to be between 8nm and 44nm, with a bimodal distribution; most fibers having an average diameter between 16nm and 20nm. The size of the fibers has been attributed to the catalyst particle dimension [27]. BSE was used to show that the spent palladium catalyst remained within the CFF itself.

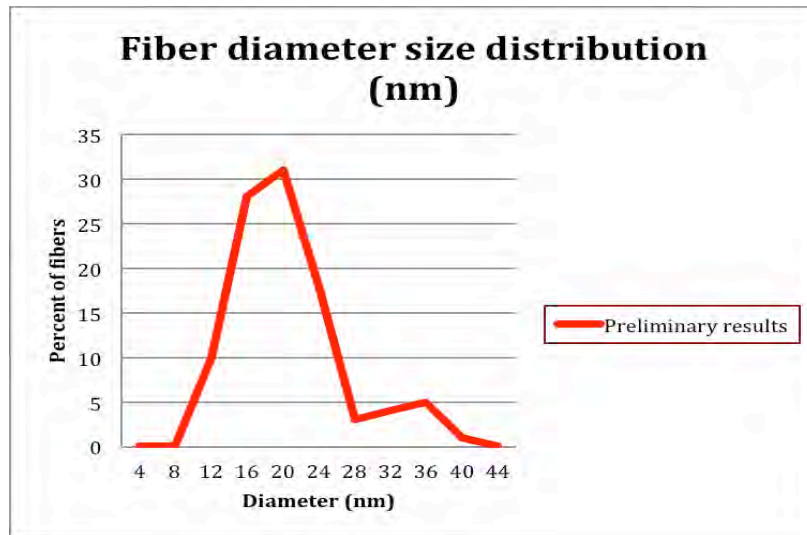


Figure 25. CFF diameter size distribution of the preliminary experimental results used as a comparison against other experimental results.

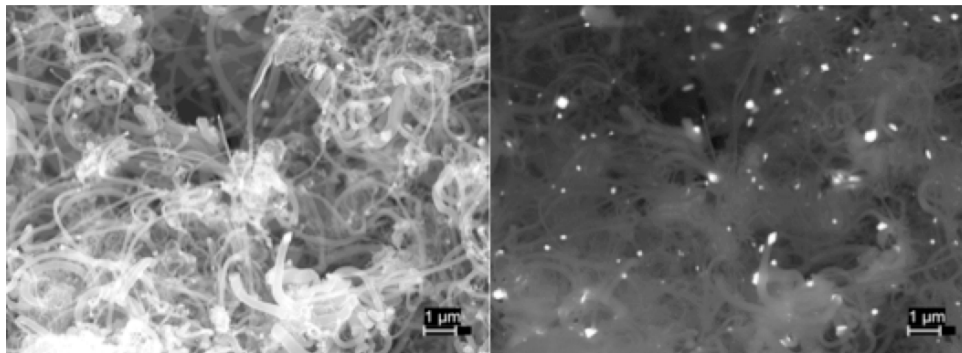


Figure 26. SEM and BSE taken of foam at 7.5K magnification. The bright regions show the palladium the remains within the foam after growth.

## 2. CFF Experiment: Without Deflector

The results of the first scaled up CFF experiment utilizing the larger mold chamber in combination with the increased gas flows and increase palladium amount, produced foam that was nonhomogeneous throughout its entirety. This experiment did not utilize a deflector or the serpentine inlet. As shown in Figure 27. the inlet region of foam showed deep grooves in the surface that lined up squarely with the inlets from the forward gas chamber. The groves appeared to be created by the gas flows velocity into the primary chamber. The texture of the foam located in the forward one third of the chamber felt consistent with the preliminary CFF experimental foam. The quality of the foams texture deteriorated past this point. Near the mid-span section of the chamber, the foam began to no longer bond with the forward section of foam and produced individual thin foam flakes. The rear of the chamber was nearly void of foam except for a few small foam flakes that appeared to grow along the sides of the chamber walls. Despite the poor consistency throughout the mold observed, the SEM results (Figure 28) show the foam fibers that were created are of similar diameter size distribution as those found in the preliminary foam experiments seen in Figure 25.

Experiment values:

- Initial palladium weight: 0.68 grams
- Final foam weight: 16.02 grams
- Foam surface area: 42.2 m<sup>2</sup>/g (results from BET analysis)
- The total weight of the foam grown was 16.02 grams.

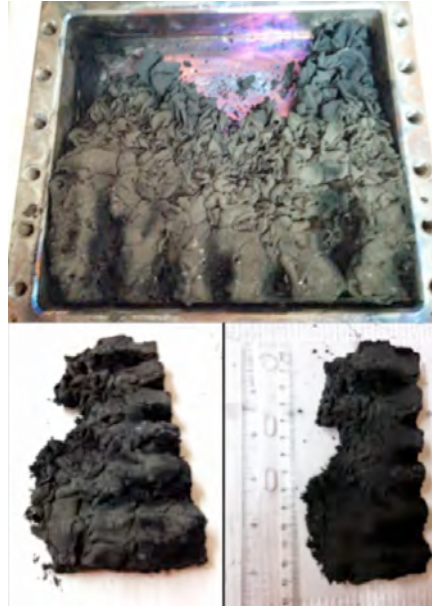


Figure 27. Scaled CFF experiment images showing the results after opening the main chamber.

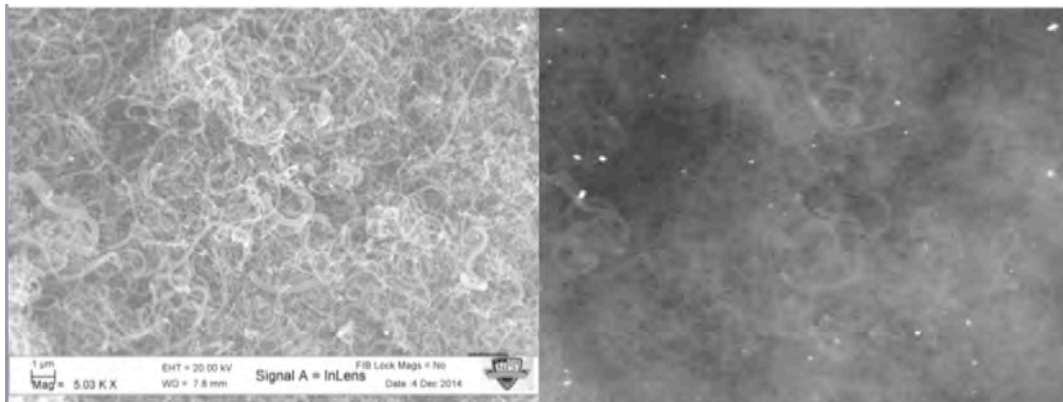


Figure 28. Left image shows an SEM image taken of the foam experiment that utilized no deflector. Right image is a BSE image taken of the same experimental results.

After the experiment conducted with no deflector just described, all experiments implemented the use of the longer serpentine inlet because it was believed that the lack of growth was a consequence of gases not reaching the growth temperature required. The use of the specific temperatures selected for the fibers growth and the need of a winding curve (serpentine) to introduce the reactive gases into the mold (shown in Figure 10)

could be explained by reviewing some fundamental concepts, such as pyrolysis and free radicals.

At high temperatures, in the presence of sufficient amounts of an oxidant, a hydrocarbon will generate gaseous  $\text{CO}_2$  and  $\text{H}_2\text{O}$ , forming no solid byproducts. However, in the absence of an oxygen, organic materials will decompose in a process known as pyrolysis, leaving carbon as end product. Other elements present in the original hydrocarbon will form gaseous byproducts and diffuse away.

Many of the forms of carbon of technological interest are formed by pyrolysis, including highly oriented pyrolytic graphite (HOPG), carbon fibers, carbon nanotubes, glassy and amorphous carbon. The growth of carbon nanotubes and nanofibers requires a high level of control during the pyrolysis process for hydrocarbon molecules to react with the catalyst, otherwise the carbon will not grow in a controlled manner and will just deposit as amorphous carbon.

The activation of the ethylene molecule by heating creates free radicals that facilitate the pyrolysis. In the chemistry, a free radical refers to an atom, molecule or ion that has unpaired electrons. Free radicals are electron-deficient species, but they are usually uncharged, so their chemistry is very different from the chemistry of even-electron or electron-deficient species. The unpaired electrons make the radicals highly reactive. The most important radical reactions are: formation, propagation and termination.

The reason why the temperature should be high during the nanofiber growth process is because the kinetic energy of the gas increases with temperature as well as the amount of radicals formed. Therefore, the serpentine shown in Figure 10 was used to force the reactive gases to heat to the reaction temperature (550 degrees C) before reaching the mold and assure the breakage of the ethylene molecule and allow the radicals to interact with catalyst particles. Moreover, the growth process is conducted at a constant flow of the reactant gas mixtures (controlled by the MFC system) to remove the unwanted byproducts. Such constant flow also avoids the generation of carbon clusters or

independent nuclei and favors the incorporation of carbon to the already growing nanofiber substrate.

The use of nitrogen gas during the growth step is meant to dilute the ethylene to prevent supersturation conditions and direct the growth to only the catalytic sites rather than forming new nuclei.

### 3. CFF Experiment: Rod Deflector ONE

The solidification of the foam generated using the stainless steel rod deflector improved slightly over the no deflector experiment. The deep grooves that had formed previously were not as prominent as seen in Figure 29. The size of the grooves had been reduced forming only small ridges in the vicinity of the gas inlets. The length of the forward solid foam section had grown to reach nearly half the length of the chamber. The small flakes were still present but now occupied the entirety of the rear region chamber floor.

Experiment values:

- Initial palladium weight: 0.5 grams
- Final foam weight: 19.12 grams
- Foam surface area: 163.2 m<sup>2</sup>/g

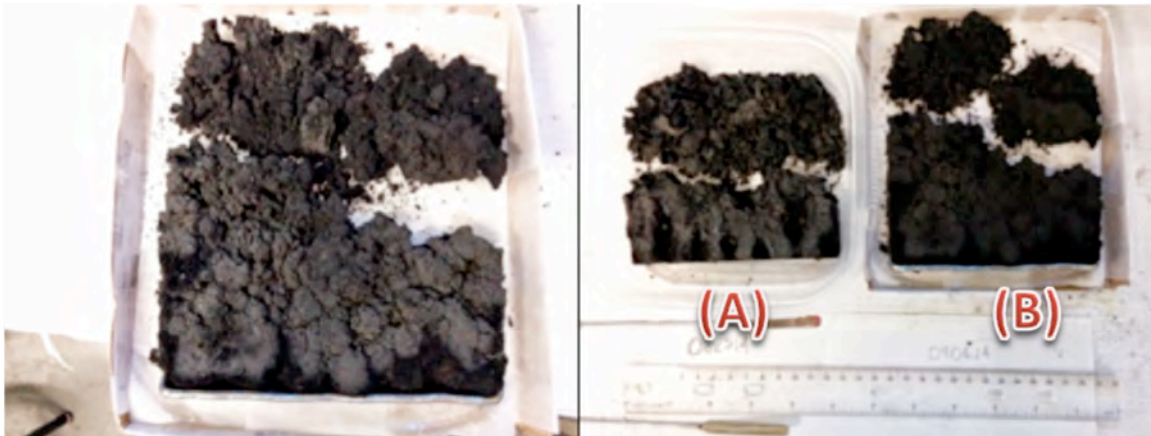


Figure 29. Left image shows foam after removal from the main chamber. Right image shows and (right) a comparison between the non-deflected (A) and deflected (B) experiments.

SEM images taken of a sample from the forward region's good foam showed the fibers ranged in diameter from 10 nm to approximately 36 nm as seen in Figure 30. BSE images of the foam sample showed light Palladium deposits remained within the generated foam. SEM and BSE results show that the fibers created were similar to the foam fibers generated during the preliminary experiments.

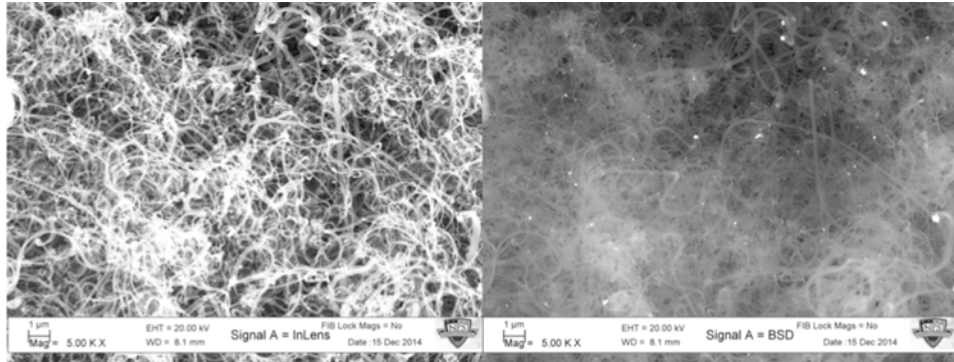


Figure 30. Left image shows an SEM image taken of the foam from Rod Deflector ONE experiment. Right image is a BSE image taken of the same experimental results.

#### 4. CFF Experiment: Foil Deflector ONE

The use of stainless steel deflector-one resulted in the first scaled experiment to create solid foam growth spanning the chamber length to the far end. The foam in the forward section of the chamber, near the gas inlets showed cavity formation, which was attributed to the inlet gas's velocity continuing to impact forward foam generation. Dispersion of the foam growth was not symmetric within the chamber. As shown in Figure 31, foam along the right half of the chamber formed along the entirety of the chamber length while that on the left side of the chamber only produced low-density foam that started forming after approximately one third of the chamber length. It is believed that the front far left inlet was partially blocked by the deflector while the one on the far right was not. This is believed to have caused the uneven growth seen within the chamber.

Experiment values:

- Initial palladium weight: 0.5 grams

- Final foam weight: 10.75 grams
- Foam surface area: 30.37 m<sup>2</sup>/g



Figure 31. Image taken of the results from Foil Deflector ONE's experiment after the main chamber was opened.

SEM and BSE images confirmed the consistent production of good CFF fiber being generated within the chamber (Figure 32). The physical characteristics of the foam fiber continue to mimic those of the successful, non-scaled preliminary experimental foam fiber having a diameter distribution spanning 16–40 nm.

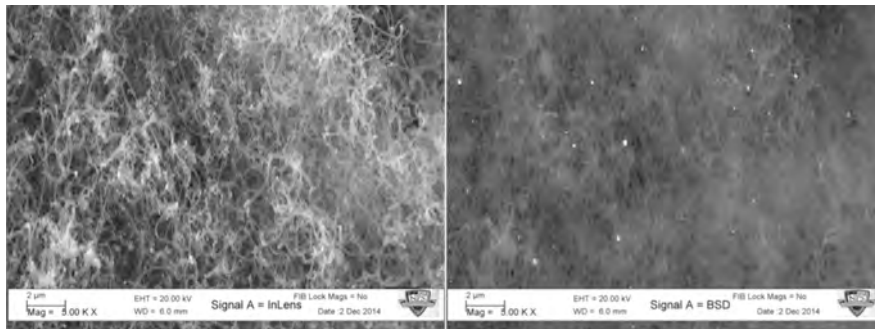


Figure 32. Left image shows an SEM image taken of the foam from Foil Deflector ONE's experiment. Right image is a BSE image taken of the same experimental results.

## 5. CFF Experiment: Foil Deflector TWO

Foam grown using Foil Deflector TWO filled the chamber with CFF of varying texture quality as shown in Figure 33. The forward chamber section's foam was nearly void of cavities and appeared consistent along the width of the chamber. Along the side regions, the foam was also of good texture quality. This good quality foam extended from the forward and side interior walls toward the center approximately one inch. Both the forward and side sections bonded together to form a solid piece of foam. The center region within the chamber, between the gap in the deflector's top section and the interior walls, produced foam of low quality texture. The foam had poor bonds to the front and side regions and crumbled easily with the application of a small force. The strength of the foam felt low compared to that of the front and side sections. The foam compressed easily, without significant resistance. The foam that generated directly beneath the gap in the deflector's top section was of lower texture quality than the front and side regions but higher than that of the foam in the center regions. This led to the decision to increase the open areas present in the deflector to allow additional precursor gases to reach the poorer foam producing regions. It was approximated that 60% of the main chamber was filled with foam of the desired texture quality.

Experiment values:

- Initial palladium weight: 0.51 grams
- Final foam weight: 12.419 grams
- Foam surface area: 111.35 m<sup>2</sup>/g



Figure 33. Left image shows Foil Deflector TWO's experiment after opening of the main chamber. Right shows the main chamber after the removal of Foil Deflector TWO.

SEM and BSE results continued to show the fiber being generated being of similar characteristic and quality as those created in the preliminary CFF experiment (Figure 34). The fiber size distribution ranged from approximately 16–40 nm.

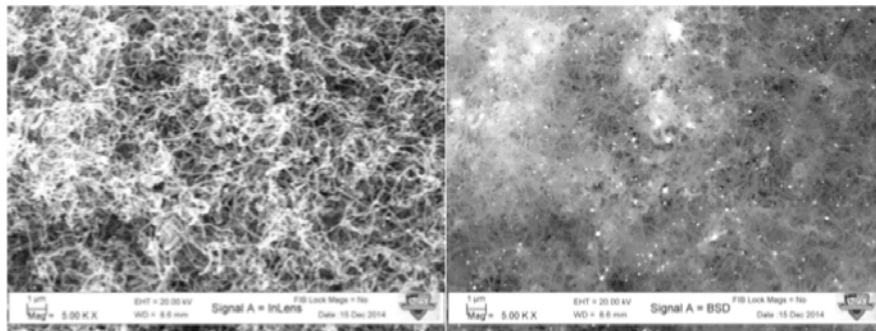


Figure 34. Left image shows an SEM image taken of the foam from Foil Deflector TWO's experiment. Right image is a BSE image taken of the same experimental results.

## 6. CFF Experiment: Foil Deflector THREE

Foil Deflector THREE's experiment increased the experimental run time from 5 to 10 hours. This was done to increase the time available for the CFF fibers to grow and observe how a change in this variable impacted the foam being generated. Modifications were also made to the deflector. The results from increasing the open area in the deflector

were mostly positive. The forward foam producing regions remained relatively constant compared to the previous experimental results. The side regions again produced good quality foam the length of the chamber. The solid, interwoven section of foam that was generated, grew in width from the front and side interior sidewalls toward the center approximately one and a half inch. The center rear region of the main mold chamber continued to generate more of the low density, poor cohesion CFF (Figure 35). This low quality foam appeared to nucleate but never becomes fully interwoven with the surrounding CFF material. The additional experiment time did not appear to significantly improve the foam generation. This supports the assumption that precursor flow control is of greater significance in the growth process.

Experiment values:

- Initial palladium weight: 0.5078 grams
- Final foam weight: 21.28 grams
- Foam surface area: 122 m<sup>2</sup>/g



Figure 35. Left image shows Foil Deflector THREE's experiment after opening of the main. Right image shows the CFF generated during the process.

SEM images verify that the perceived higher quality regions of foam being generated are of comparable physical properties of the early production foams we are

attempting to reproduce in scaled quantities having a fiber diameter size distribution between 8–24 nm (Figure 36).

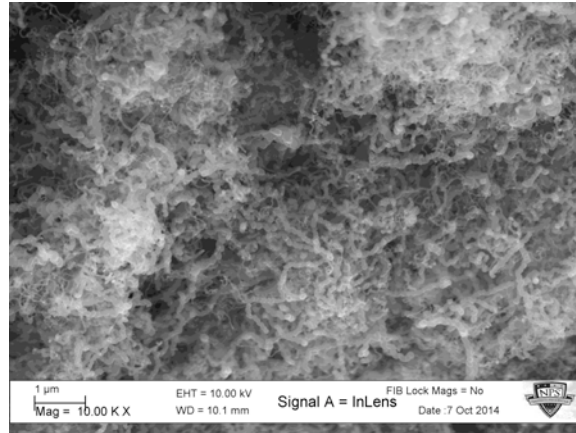


Figure 36. SEM image taken from sample 103014.

## 7. CFF Experiment: Foil Deflector FOUR

Foil Deflector FOUR's experiment utilized the addition of Tungsten Oxide (WO<sub>3</sub>) power (0.0626 grams) combined with the palladium catalyst. The WO<sub>3</sub> addition aimed to increase the CFF's material strength as was done in other related experimental studies [31]. The experiment was again allowed to run for 10 hours to increase the time available for CFF growth. Changes made to the deflector dimensions increased the forward gap to allow additional flow to enter the front of the main chamber. Changes were also made to the deflectors cover to decrease the open area in the rear center of the cover. The combination of the changes had an overall poor effect on the foam that was generated (Figure 37). The foam's texture in the forward and side regions, which had previously been of good quality, no longer felt elastic. The foam generated was now brittle and stiff. The foam in the center rear region was also flaky. Of positive note, the size of the center rear region of foam that did not combine into the single solid foam of the front and side regions decreased slightly from the previous experiment, increasing the overall size of the single solid foam piece.

Analysis of the experiments SEM images revealed that the addition of tungsten oxide powder had an observable impact on the foam's fiber diameter (Figure 38). The

tungsten oxide had the effect of decreasing the individual fibers diameter distribution as observed in Figure 39. The tungsten oxide's negative impact to the foams texture and elasticity preclude its future use in this thesis's future experiments, as precursor of WS<sub>2</sub>. Future efforts will include this secondary phase, a known shock absorber [3, 31].

Experiment values:

- Initial palladium weight: 0.5012 grams
- Tungsten Oxide weight: 0.0626 grams
- Final foam weight: 21.28 grams
- Foam surface area: 122.13 m<sup>2</sup>/g



Figure 37. Left image shows Foil Deflector FOUR's experiment after opening of the main chamber. Right image shows the removed CFF block after removal from the main chamber.

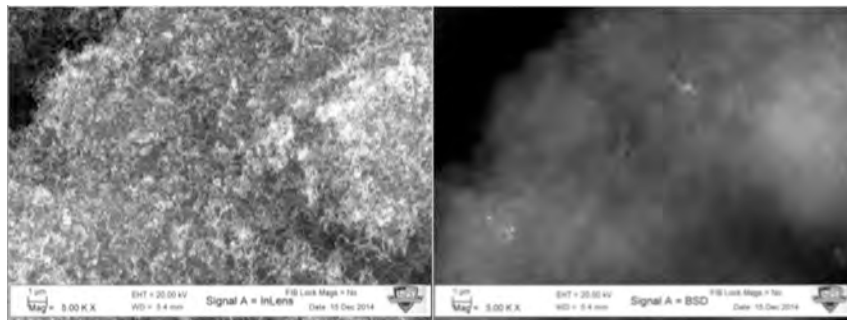


Figure 38. Left image shows an SEM image taken of the foam from Foil Deflector FOUR's experiment. Right image is a BSE image taken of the same experimental results.

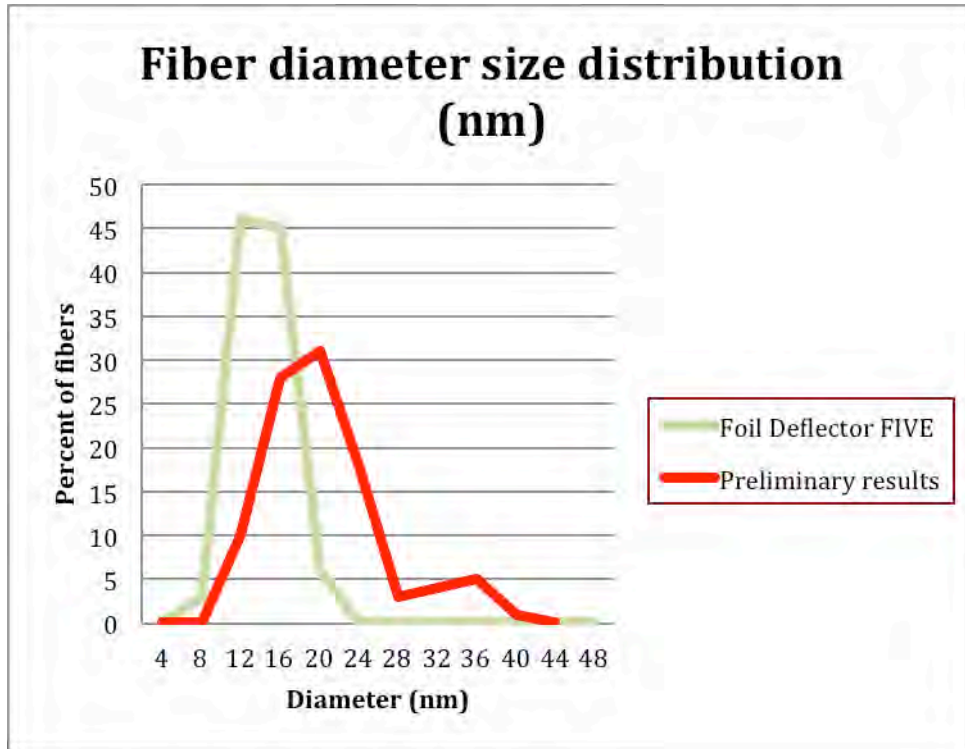


Figure 39. Smaller fiber diameters observed due to the inclusion of tungsten oxide.

## 8. CFF Experiment: Foil Deflector FIVE

Foil Deflector FIVE's experiment returned to deflector three's dimensions with only minor modifications made to the rear center gap section. The gap was decreased in size utilizing a cover. This cover created two parallel 1/4 x 1-inch slits and decreased the amount of open area in the cover's rear center region (Figure 40). This experiment was run for 5 hours. After cooling, flow direction was reversed by switching the gas inlet and outlet lines and the experiment resumed for the additional 5 hours. This was done to provide the rear section of chamber fresh, unspoiled gas flows. The premise for this action was that the palladium remaining in the rear chamber would then grow similarly to that of the palladium within the front of the chamber. Opening the chamber revealed that the rear center region despite the directional change continued to produce the poor bonding, low texture quality foam. It was observed that the CFF that formed in the rear sections began to cover the outer chamber gas outlets. The closure of these outer gas outlets forces the exhaust gases to flow entirely through the remaining center gas outlets.

This exhaust is believed to be enough to stop the CFF generation process. It is now believed once individual nucleation of the foam generation process is interrupted, there seems to be no recovering likely due to the formation of carbon caps, which form over the palladium catalyst. This conclusion is based on the observation of providing the remaining palladium in the rear of the chamber with the same gas flows as the beginning of the experiment and continuing to see the poor foam unchanged despite the new direction of gas flow.

Experiment values:

- Initial palladium weight: 0.5037 grams
- Final foam weight: 26.86 grams
- Foam surface area: 94.58 m<sup>2</sup>/g

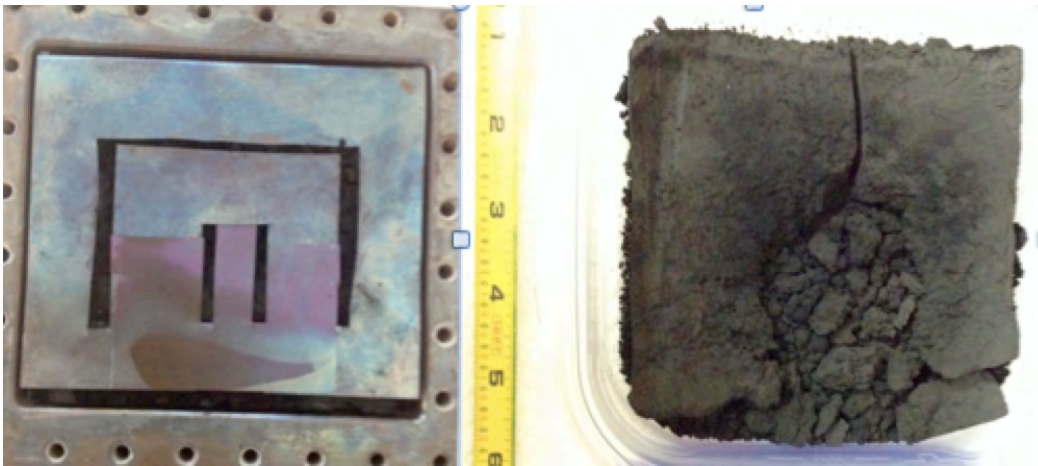


Figure 40. Left image shows Foil Deflector FIVE's experiment after opening of the main chamber. Right image shows the removed foam block after removal from the main chamber.

SEM and BSE images (Figure 41) shows consistent good foam characteristics are being produced in the regions where good foam texture is observed.

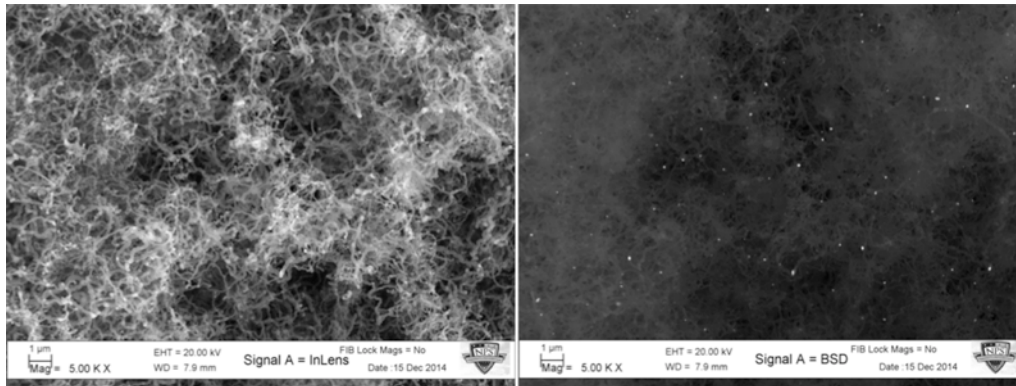


Figure 41. Left image shows an SEM image taken of the foam from Foil Deflector FIVE's experiment. Right image is a BSE image taken of the same experimental results.

## 9. CFF Experiment: Foil Deflector SIX

A rear stainless steel deflector was used in addition to the deflector set up from Foil Deflector FIVE's experiment (Figure 43). The new rear deflector addition is held in place using the rear prongs that hold the foam base in place during the experiment. The additional deflector was added to prevent the gas outlets from being clogged with newly generated CFF, which then could change gas flows and possibly cause exhaust gases to become condensed in the main chamber. The experiment ran continuously for 10 hours without changes in the gas flow direction.

The foam generated in Foil Deflector SIX's experiment formed a solid interwoven foam block (Figure 44). The addition of the rear deflector permitted the generation of the good quality textured CFF to form in all regions, including the center rear region of the main chamber. All regions of the chamber were interwoven, which allowed for the removal of the block as a single unit (Figure 45). Despite the appearance of minor CFF nucleation clusters that formed atop the interwoven mat below, the experiment was determined to have met the objectives set forth in the thesis.

SEM images taken from a sample of the CFF show the size characteristics of the CFF fibers closely match those obtained from the preliminary experiments (Figure 46). This is important because it indicates that despite the increased scale of the generated foam, the foam fibers produced continue to have the same desired physical characteristics

as those produced in the earlier preliminary experiments. A table summarizing all experimental variables and results are provided in Table 2.

Additional ANSYS modeling was conducted to show the new precursor flow paths within the chamber due to the addition of Foil Deflector SIX. As shown in Figure 42 the flow paths travel around the deflector creating several additional fresh flow sources that now reach all regions of the chamber. As CFF generation occurs, it will start to obstruct lower flow paths shown within the forward region of the model, these lower flow paths will begin to slow due to the newly formed nanofoam obstructions. Precursor flows will redistribute to other unobstructed pathways. These other pathways provide continuous precursor flow to all regions of the chamber.

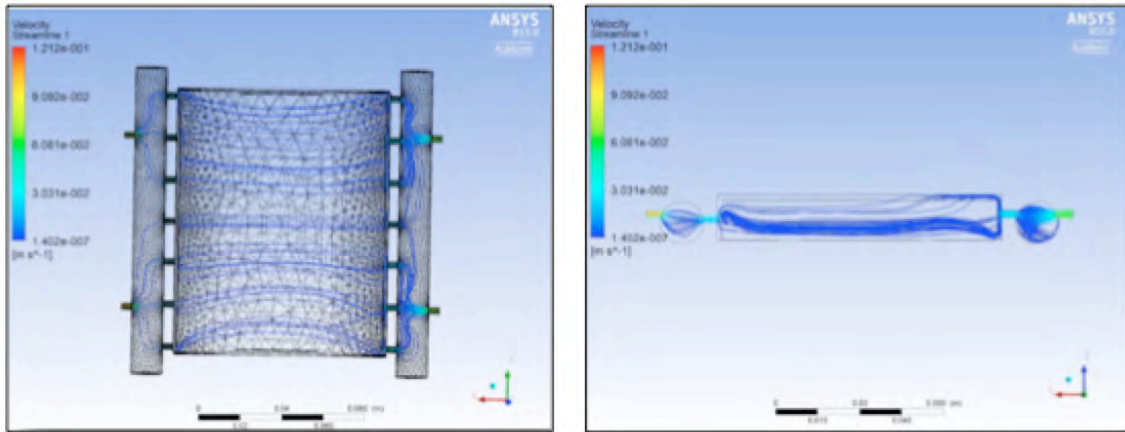


Figure 42. ANSYS modeling of the mold chamber utilizing Foil Deflector SIX shows the modified flow paths within the chamber.

Experiment values:

- Initial palladium weight: 0.5064 grams
- Final foam weight: 19.69 grams
- Foam surface area: 58.52 m<sup>2</sup>/g

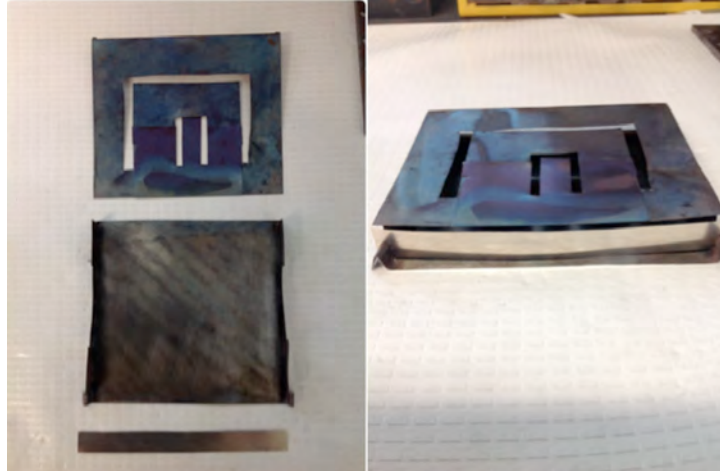


Figure 43. Left image shows the completely disassembled Deflector SIX from the experiment. Right image shows a rear view of the assembled deflector.



Figure 44. Image shows Foil Deflector SIX experiment growth after opening of the main chamber.



Figure 45. Left image shows a forward view of the CFF block generated during Foil Deflector SIX's experiment and placed atop the main chamber after removal. Right image shows a rear view of the results.

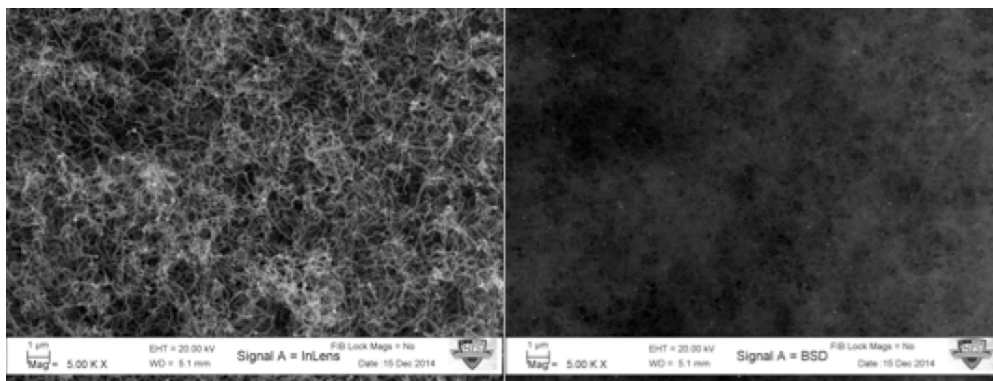


Figure 46. SEM and BSE images taken from a sample of the CFF block generated in Foil Deflector SIX's experiment.

Table 2. Summary of all experimental variables.

Experiment #	Name	Experimental variables						Experimental results		
		Deflector	Catalyst weight	Gas Flow (SCCM)			Time	Surface Area (m <sup>2</sup> /g)	Percent of chamber filled (%)	Final foam weight (g)
				N <sub>2</sub>	O <sub>2</sub>	C <sub>2</sub> H <sub>4</sub>				
1	082514	N/A	(Pd) 0.68 g	100	15	15	5 hr	42.2	33	16.02
2	090314	Rod Deflector ONE	(Pd) 0.5 g	300	45	45	5 hr	163.2	50	19.12
3	092414	Foil Deflector ONE	(Pd) 0.5 g	300	45	45	5 hr	30.37	55	10.75
4	093014	Foil Deflector TWO	(Pd) 0.51 g	300	45	45	5 hr	11.53	60	12.419
5	100314	Foil Deflector THREE	(Pd) 0.5078 g	300	45	45	10 hr	122	75	21.28
6	100914	Foil Deflector FOUR	(Pd) 0.5012 g (WO <sub>3</sub> ) 0.0626 g	300	45	45	10 hr	122.13	60	20.54
7	102114	Foil Deflector FIVE	(Pd) 0.5037 g	300	45	45	10 hr + 5 hr	94.58	85	26.86
8	103114	Foil Deflector SIX	(Pd) 0.5064 g	300	45	45	10 hr	58.52	100	19.69

The analysis of the surface area values in Table 2 show that the samples that nearly or completely filled the mold have intermediate values (in the order of 50–100 m<sup>2</sup>/g). These results can be explained, in one hand, by the fact that carbon nanostructures with higher surface areas will have more empty space in between fibers, not enough to interweave and generate a foam. On the other hand, samples with small surface areas will have such a dense structure, that the fibers will lock each other in position and will not present the desired mechanical properties. It is worth noting that the relative density of the foam that completely filled the mold is 0.245, similar to balsa wood [5].

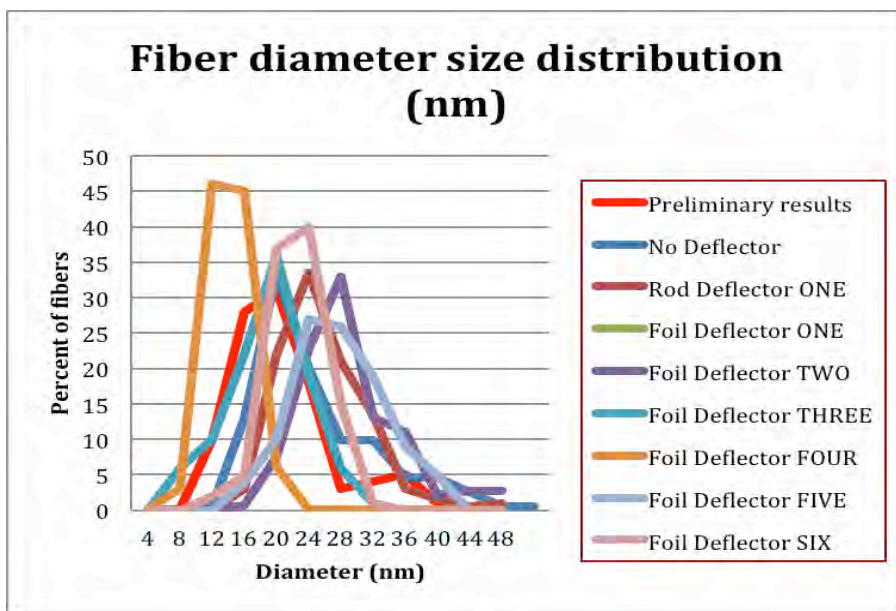


Figure 47. Consolidated diameter distribution results from all CFF experiments.

The consolidated diameter results shown in Figure 47 reveal that the CFF material being generated (with the exception of the tungsten oxide Deflector FOUR experiment) all had similar bimodal diameter size distributions. Quality control processes can be created from this knowledge. Diameter distribution measurements can act as a standard that can gauge the quality of the nanofoam being fabricated. The most effective experiment, Deflector SIX, which was able to fill the mold, had an average diameter size of 24 nm, with almost no fibers below 15 nm or greater than 32 nm. Larger diameters seem to form aggregates rather than foams.

## F. CATALYST RECOVERY: SUMMARY OF FINDINGS

SEM and BSE images were taken of the samples after having gone through the palladium extraction procedure at locations near the outer edge of the surface and at the interior of the sample (Figure 48). The BSE images were utilized to distinguish the palladium particles from the carbon fibers. These images were then analyzed using the software, Image J, to measure particle sizes and compare the particle density remaining in the foam after going through the individual extraction solutions [30].

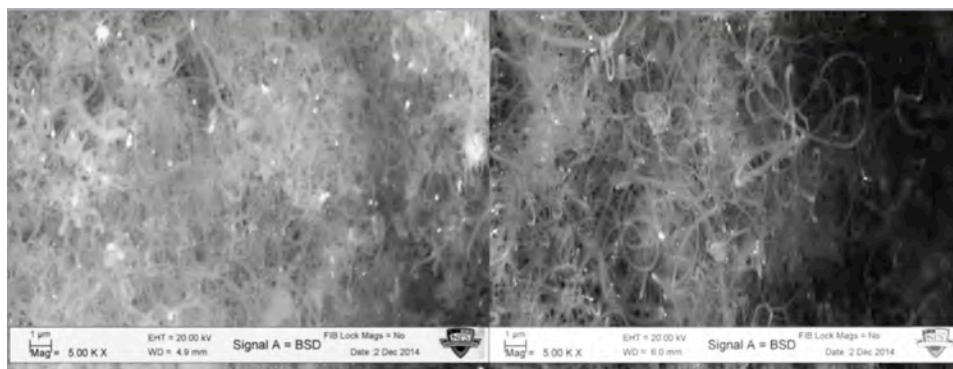


Figure 48. BSE images taken of samples after the palladium recovery procedure. Left image shows solution 1 sample and right image shows solution 2 sample.

### 1. Interior region analysis

Comparing the particle size distribution between the two solutions revealed that solution 2, which was comprised of an aqueous solution, hydrochloric acid (10%) and peroxide (5%) had the greatest impact at dissolving palladium. Figure 49 shows fewer large palladium particles (particles greater than 12 nm diameter) were present in the solution 2 sample's interior region when compared to solution 1 sample's interior region. The solution 2 sample's interior on the other hand had a significantly greater number of smaller particles (particles less than 12 nm diameter) in this region. This is likely due to larger particle breaking ups and forming numerous smaller particles that never fully dissolve but remained in the CFF sample.

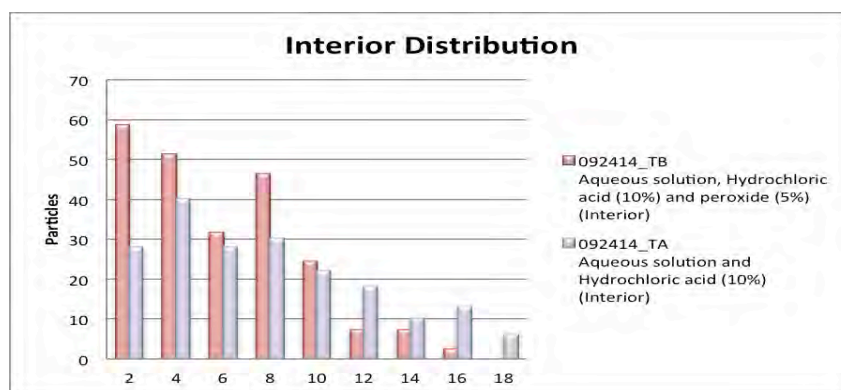


Figure 49. Palladium catalyst particle size distribution of the interior region of sample specimen taken after recovery method procedure.

## 2. Exterior region analysis

Figure 50 shows the particle distribution of each solutions exterior region. The solution 2 sample exterior region contained a greater number of larger particles than the solution 1 sample. Both had significantly fewer large particles than were found in the interior region. This increase in the number of large particles found in the exterior region is likely due to a combination of larger particle breakups and particle migration from the interior region. Both exterior sample distributions showed significantly greater numbers of smaller palladium particles also likely due to the partially dissolved particles migrating out of the foam.

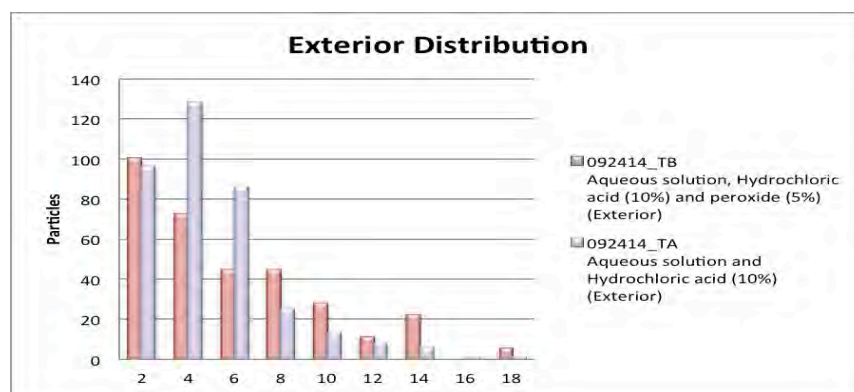


Figure 50. Palladium catalyst particle size distribution of the exterior region of sample specimen taken after recovery method procedure.

The spent catalyst recovery experiment demonstrated a successful process that could be used as a method to recover the valuable palladium used in the CFF generation. It also shows that the addition of the peroxide resulted in greater dissolution of the palladium. Additional time as well as an increase in the amount of solution would likely improve the results obtained further.

## IV. CONCLUSION

The primary goal of this research was to show that the CFF production process could be scaled in order to fabricate mechanically robust, homogenous foam samples that meet dimensions adequate for further testing. CFF materials have important material characteristics, such as significant shock absorption properties, that make this effort worthwhile.

Scale up of the production process required the design and manufacture of a CFF chamber. The chamber created for this thesis was capable of facilitating and enabling the growth model variable conditions (precursor flow, constrained growth area, temperature, and time) necessary to enable the generation of carbon nanofibers. Through the control of these variables, a homogenous, interwoven CFF mat was successfully created using the catalyst palladium and carbon rich gas ethylene. SEM, BET, and BSE characterization techniques were conducted on the scaled experimental samples to confirm that the foams created during these experiments were of similar quality as those created during previous experimental research.

Analysis of the CFF growth variables and their impact on the generated foam samples showed that precursor flow interaction with the catalyst had a greater impact on the foam development than time. This variable was successfully controlled throughout the chamber by the utilization of a stainless steel deflector capable of directing sufficient precursor gas flows to all chamber regions. This flow rate was sufficient enough to prevent the formation of carbon caps, which can encapsulate the palladium catalyst particles and cease the growth mechanism by preventing the decomposition of hydrocarbon gas. Moreover, the temperature and velocity of the gases were key for successful CFF growth. In this study, the use of a serpentine was indispensable to reach those optimal conditions.

ANSYS modeling can be used to simulate initial gas flows and provide guidance for deflector design. However, once the fibers start growing, these models are no longer

valid since the fibers obstruct and change the initial gas flow paths and drastically change the conditions inside the mold.

Spent catalyst recovery techniques were researched and from this research, an experiment was created to extract the palladium from the CFF. This test used acidic solutions to dissolve the spent catalyst without damaging the CFF material. BSE image analysis showed the successful dissolution of the palladium catalyst from within the CFF. This successful experiment validated the technique as a viable way to reduce costs of CFF fabrication by recovering the spent catalyst for reutilization.

Overall, this research has successfully demonstrated the CoFFiN fabrication method's scalability for the bulk generation of carbon nanofiber foam mats, validating the hypothesis presented in Chapter I.

# APPENDIX

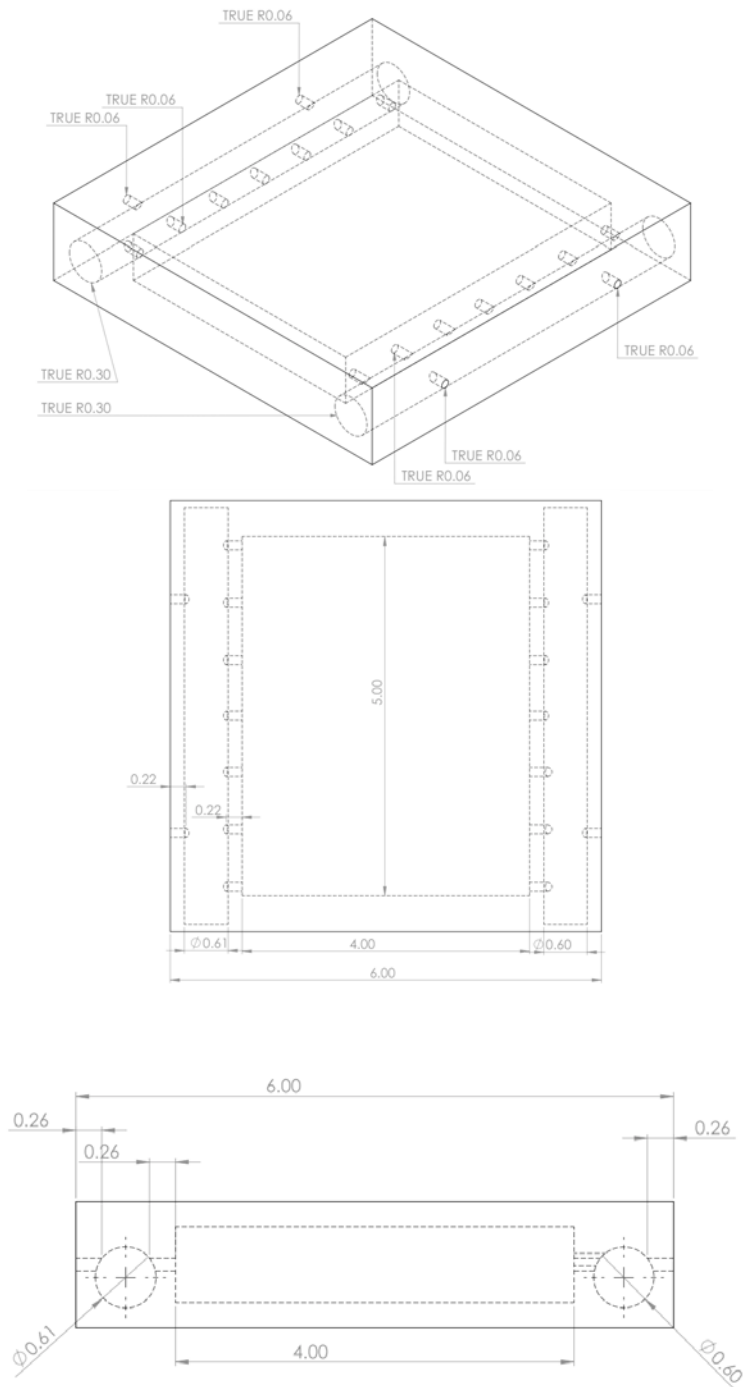


Figure 51. SOLIDWORKS renderings of the new mold chamber design.

THIS PAGE INTENTIONALLY LEFT BLANK

## LIST OF REFERENCES

- [1] C. Dean, "The modern warrior's combat load: dismounted operations in Afghanistan April - May 2003," U.S. Army Center for Army Lessons Learned, pp. 1–119, May 2003.
- [2] Y. Satoa et al., "Reinforcement of rubber using radial single-walled carbon nanotube soot and its shock dampening properties," *Carbon*, vol. 46, pp. 1509–1512, Sep. 2008.
- [3] C. C. Luhrs et al., "IF-WS<sub>2</sub>/Nanostructured carbon hybrids generation and their characterization," *Inorganics*, vol. 2, pp. 211–232, Mar. 2014.
- [4] A. Mousavi et al., "Mechanical and electrical characterization of entangled networks of carbon nanofibers," *Materials*, vol. 7, pp. 4845–4853, Jun. 2014.
- [5] D. Daskam, "Mechanical and electrical characterization of novel carbon nano fiber ultralow density foam," M.S. thesis, Mechanical. Engineering Dept., N.P.S. Monterey, CA, 2013.
- [6] N. Chakrapani, "Capillarity-driven assembly of two-dimensional cellular carbon nanotube foams," in *Proc. Natl. Acad. Sci. U.S.A.*, vol. 101, pp. 4009–4012, Mar. 2004.
- [7] D. Futaba et al., "Shape-engineerable and highly densely packed single-walled carbon nanotubes and their application as super-capacitor electrodes," *Nature Materials*, vol. 5, pp. 987–994, Nov. 2006.
- [8] M. Kumar and Y. Ando, "Chemical vapor deposition of carbon nanotubes: A review on growth mechanism and mass production," *Journal of Nanoscience and Nanotechnology*, vol. 10, pp. 3739–3758, Jan. 2010.
- [9] D. Futaba, "Shape-engineerable and highly densely packed single-walled carbon nanotubes and their application as super-capacitor electrodes," *Nat. Mater*, vol. 5, pp. 987–994, Dec. 2006.
- [10] W. Hung et al., "Rapid prototyping of three-dimensional microstructures from multiwalled carbon nanotubes," *Appl. Phys. Lett.*, vol. 91, p. 093121, Aug. 2007.
- [11] M. Atwater et al., "Direct synthesis and characterization of a nonwoven structure comprised of carbon nanofibers," *Carbon*, vol. 57, pp. 363–370, Jun. 2013.
- [12] M. Atwater et al., "The effect of powder sintering on the palladium-catalyzed formation of carbon nanofibers from ethylene-oxygen mixtures," *Carbon*, vol. 48, pp. 1932–1938, June 2010.

- [13] C. Luhrs et al., “Generation of carbon nanofilaments on carbon fibers at 550 degrees C,” *Carbon*, vol. 47, pp. 3071–3078, Nov. 2009.
- [14] Dassault Systèmes SOLIDWORKS Corp., “SOLIDWORKS,” Vélizy-Villacoublay, France, 2015.
- [15] P. Smith and J. Cashman, “ANSYS-Computational Fluid Dynamics (CFD) Software,” Cecil Township, Pennsylvania, 2015.
- [16] C. C. Luhrs et al., “Fabrication of a low density carbon fiber foam and its characterization as a strain gauge,” *Materials*, vol. 7, pp. 3699–3714, May 2014.
- [17] Ş Sariođlan, “Recovery of palladium from spent activated carbon-supported palladium catalysts,” *Platinum Metals Review*, vol. 57, pp. 289–296, Oct. 2013.
- [18] M. Barakat et al., “Hydrometallurgical recovery of nano-palladium from spent catalyst,” *Mineral Process. J.*, vol. 2, pp. 31–36, Mar. 2009.
- [19] R. Jasra et al., “Process for recovery of palladium from spent catalyst,” U.S. Patent 7,473,406, January 6, 2009.
- [20] *Handbook of Carbon, Graphite, Diamond, and Fullerenes*, Noyes Publications, Park Ridge, N.J., 1993.
- [21] D. Jones, “Science of fullerenes and carbon nanotubes,” *Nature*, vol. 381, pp. 384–384, May 1996.
- [22] A. Rode et al., “Unconventional magnetism in all-carbon nanofoam,” *Phys. Rev. B*, vol. 70, p. 054407, Aug. 2004.
- [23] O. Nerushev et al., “Particle size dependence and model for iron-catalyzed growth of carbon nanotubes by thermal CVD,” *J. Appl. Phys.*, vol. 93, p. 4185, Mar. 2003.
- [24] R. Morjan et al., “Growth of carbon nanotubes from C60,” *Appl. Phys. A*, vol. 78, p. 235, Feb. 2004.
- [25] M. Rummeli et al., “Novel catalysts, room temperature, and the importance of oxygen for the synthesis of single-walled carbon nanotubes,” *Nano Lett.*, vol. 5, p. 1209, May 2005.
- [26] F. Ding et al., “The importance of strong carbon–metal adhesion for catalytic nucleation of single-walled carbon nanotubes,” *Nano Lett.*, vol. 8, pp. 463–468, Dec. 2007.
- [27] G. Cao, *Nanostructures & Nanomaterials, Synthesis, Properties & Applications*. London: Imperial College Press, 2004.

- [28] K. Kolasinski, "Catalytic growth of nanowires: vapor-liquid-solid, vapor-solid-solid, solution-liquid-solid and solid-liquid-solid growth," *Current Opinion in Solid State and Materials Science*, vol. 10, pp. 182-191, Jun. 2006.
- [29] V. Dubrovskii et al., "Theoretical analysis of the vapor-liquid-solid mechanism of nanowire growth during molecular beam epitaxy," *Physical Review E*, vol. 73, Feb. 2006.
- [30] W. Rasband, "Image J," Nat. Institutes of Health, Bethesda, Maryland, 1997-2014.
- [31] A. Maxson, "Novel synthesis and characterization of inorganic fullerene type WS<sub>2</sub> and graphene hybrids," M.S. thesis, Mechanical Engineering Dept., N.P.S. Monterey, CA, 2013.

THIS PAGE INTENTIONALLY LEFT BLANK

## **INITIAL DISTRIBUTION LIST**

1. Defense Technical Information Center  
Ft. Belvoir, Virginia
2. Dudley Knox Library  
Naval Postgraduate School  
Monterey, California